UNIVERSIDAD AUTONOMA DE MADRID

ESCUELA POLITECNICA SUPERIOR

Grado en Ingeniería de Tecnologías y Servicios de Telecomunicación

TRABAJO FIN DE GRADO

DESIGN OF AN ORTHOMODE OF X-BAND SATELLITE COMMUNICATIONS FOR ORTHOGONALLY POLARIZED SIGNAL DISCRIMINATION

Álvaro Pérez Ortega
Tutor: Jorge A. Ruiz Cruz

Junio 2015

DISEÑO DE UN ORTOMODO EN BANDA X DE COMUNICACIONES POR SATÉLITE PARA SEPARACIÓN DE SEÑALES POLARIZADAS ORTOGONALMENTE

Autor: Álvaro Pérez Ortega
Tutor: Jorge A. Ruiz Cruz

Grupo de Radiofrecuencia: Circuitos, Antenas y Sistemas (RFCAS)
Dpto. de Tecnología Electrónica y de las Comunicaciones
Escuela Politécnica Superior
Universidad Autónoma de Madrid
Junio 2015

Abstract

Ortho-Mode Transducers (OMTs) are passive microwave devices whose function is to discriminate between two orthogonal signals received by dual-polarization antenna systems. They can also be used in transmitters, combining these signals and routing them to the antenna.

These devices are frequently found in environments such as satellite communication systems, radio-astronomy or defense. Their usage in telecommunication systems allows to double the capacity of the system, since two different signals can be transmitted or received in the same frequency range as long as they are associated to different orthogonal polarizations. However, despite of the usefulness of these devices during the last decades, they are not widely dealt with in the literature.

The main objective of this project is to develop a narrowband ortho-mode transducer in rectangular waveguide technology that presents a moderately good performance within the X-Band frequencies. In order to design these devices, a good comprehension of some concepts about electromagnetic theory and waveguide analysis is required. Additionally, a survey including different OMT configurations will be presented, which will help to understand the use of certain structures (irises, tapper sections, septum...) on these devices.

Once a solid background for the project has been built the design process will be approached, making use of programs such as CST Microwave Studio (Computer Simulation Technology) and MATLAB to address an optimization cycle that will lead to our final OMT design.

Resumen

Los Transductores de Modos Ortogonales (OMTs, Ortho-Mode Transducers) son dispositivos pasivos de microondas cuya función es separar las dos señales individuales que son recibidas en sistemas con antenas de polarización dual. Por otra parte, éstos también pueden ser usados en transmisores, combinando estas dos señales y transmitiéndolas a la antena.

Estos dispositivos se encuentran frequentemente en entornos tales como los sistemas de comunicación por satélite, aplicaciones de radio-astronomía o defensa. Su uso en estos sistemas permite doblar la capacidad del enlace, haciendo que dos señales distintas puedan ser transmitidas o recibidas en la misma banda de frecuencia siempre y cuando éstas esten polarizadas ortogonalmente. No obstante, a pesar de la gran utilidad demostrada por estos dispositivos durante los últimos años, no son ampliamente tratados en la literatura.

El objetivo principal de este proyecto es desarrollar un transductor de modos ortogonales de banda estrecha en teconología de guía de onda rectangular que presente un comportamiento moderadamente bueno dentro de las frequencias de banda X. Para poder diseñar este dispositivo se requiere una buena comprensión de algunos conceptos teóricos de electromagnetismo y de análisis de guías de onda. Además se presentará un estudio que incluye diferentes configuraciones de OMTs, lo cuál ayudará a entender el uso de diferentes estructuras (irises, secciones transformadoras, septum...) en estos dispositivos. Una vez que se haya establecido el contexto dentro del cual se englobará el proyecto, se comenzará el proceso de diseño, haciendo uso de programas tales como CST Microwave Studio (Computer Simulation Technology) y MATLAB para abordar un ciclo de optimizaciones que darán lugar al diseño final de nuestro OMT.

Key Words/Palabras Clave

English

Ortho-Mode transducer, OMT, Rectangular waveguide, Septum, Iris, Narrowband, Polarization, S-parameters, S-Matrix, Microwave device, Radio Frequency, Microwave engineering.

Español

Transductor de Modos Ortogonales, OMT, Guía de onda rectangular, Septum, Iris, Banda estrecha, Polarización, Parámetros S, Matriz S, Dispositivo de microondas, Radio Frecuencia, Ingeniería de microondas.

Contents

List of Figures

List of Tables

Chapter 1

Introduction

1.1 Motivation

The *Ortho-Mode Transducer* (OMT) is a key component in numerous communication systems nowadays. This results from the fact that employing OMTs in the feed networks allows these antenna systems to perform more efficiently over their bandwidths, providing additionally enhanced capacity and versatility. These devices are frequently found in fields ranging from radio-astronomy to defense, since the dual-polarization is an essential tool in all these broadband applications. Its location in an RF feed chain system is right after the antenna, making the dual-polarized signal travel through the OMT, which discriminates between the orthogonal components and serves the two different signals at its output ports. This process is shown in Figure 1.1.

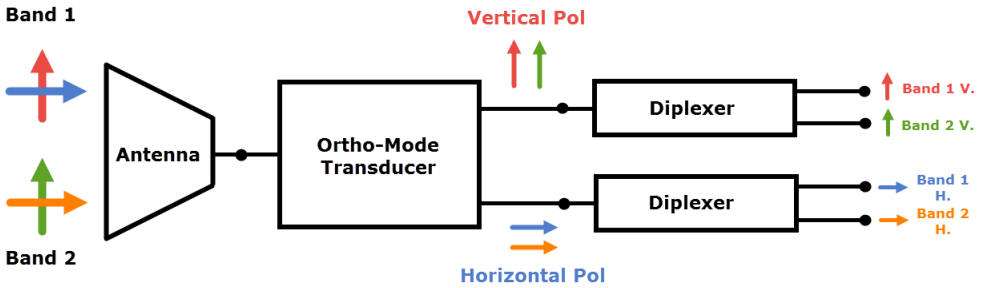

Figure 1.1: Diagram of antenna satellite communication system.

As the reader might have noticed in the figure, this configuration operates over two different frequency bands. This is actually quite common in satellite communication systems, with links ranging from 1 GHz to 30 GHz.

Needless to say that OMTs are bidirectional devices, i.e. they can also work in the opposite direction. The diagram will be exactly the same as before for transmitters. The two input signals will be fed through the single-mode ports, being combined through the OMT into the common port while maintaining them uncoupled due to the orthogonal polarization.

1.2 Goals and structure of the document

The main objective of this work is to carry out an study of the operation and the components of an OMT, and later on being able to design and simulate a fully functional OMT capable of performing moderately well within X-band frequencies. More specific requisites for the design will be presented later on the document.

Due to the extent and nature of the project, the document is presented in four parts.

First, general theory of rectangular waveguides is described as well as some basic concepts applying to every electromagnetic structure. A stronger focus is made on the modes within this waveguides as well as discontinuities and symmetries that later on will shed some light on the functioning on OMTs.

Secondly, as OMTs are not widely treated in the literature, a light survey about different designs and configurations will take place, giving the reader some understanding about the development of these structures during the last years.

Before jumping into the design process, a small chapter about the tools and techniques used for the OMT development will be presented, along with a brief description of the designing process itself.

Finally, as the last chapter, the design process of the OMT will be performed. This will include the construction of the main structure (i.e. ports, transformers...) as well as the simulations of each stage and a final optimization cycle to fulfill the specifications set for the device.

Chapter 2

Theoretical Background

2.1 Motivation

As the first chapter of the document, this theoretical introduction aims to build a solid background for the reader to fully understand the upcoming chapters and sections. However, its intention is not to present an in-depth study of electromagnetism or telecommunication systems, but to summarize and familiarize the reader with the key concepts of electromagnetic fields in waveguides as well as its theory and design.

Among the different waveguide technologies encountered in the modern communication systems, the rectangular waveguide is used in many of them; in particular in satellite systems, radio-astronomy, and general telecommunication systems working in the upper microwave and millimeter wave frequency bands. This is mainly due to the simplicity of its geometry, low losses and its capacity to perform fairly well in high power networks.

Within this context, the next sections will specially focus on waveguide discontinuities and how to use the symmetry planes of TE/TM modes to understand them and, later on, make use of this in the designing phase. Some elemental concepts might be needed in order to thoroughly comprehend the following explanations; as a reminder, these can be found in basic handbooks such as [1],[2] and [3].

2.2 Field pattern and symmetry properties of the TE/TM modes in rectangular waveguides

Each mode has a unique cross-sectional distribution of its electric and magnetic field, which remains the same along the uniform waveguide. These unique field patterns hold certain symmetry properties, which will be key to analyze if they will be excited in certain waveguide discontinuities.

Now, we will express the components of the electric and magnetic fields using a reference system located at the left-lower corner of the waveguide, as shown in Figure 2.1. The equations will end up as follows:

TE Modes	TM Modes
$E_x = \frac{j\omega\mu}{k_{c^2}}\frac{n\pi}{b}A\cos(\frac{m\pi x}{a})\sin(\frac{n\pi y}{b})e^{-\gamma z}$	$E_x = \frac{-\gamma}{k_{c^2}}\frac{m\pi}{a}A\cos(\frac{m\pi x}{a})\sin(\frac{n\pi y}{b})e^{-\gamma z}$
$E_y = \frac{-j\omega\mu}{k_{c^2}}\frac{m\pi}{a}A\sin(\frac{m\pi x}{a})\cos(\frac{n\pi y}{b})e^{-\gamma z}$	$E_y = \frac{-\gamma}{k_{c^2}}\frac{n\pi}{b}A\sin(\frac{m\pi x}{a})\cos(\frac{n\pi y}{b})e^{-\gamma z}$
$H_x = \frac{\gamma}{k_{c^2}}\frac{m\pi}{a}A\sin(\frac{m\pi x}{a})\cos(\frac{n\pi y}{b})e^{-\gamma z}$	$H_x = \frac{j\omega\epsilon}{k_{c^2}}\frac{n\pi}{b}A\sin(\frac{m\pi x}{a})\cos(\frac{n\pi y}{b})e^{-\gamma z}$
$H_y = \frac{\gamma}{k_{c^2}}\frac{n\pi}{b}A\cos(\frac{m\pi x}{a})\sin(\frac{n\pi y}{b})e^{-\gamma z}$	$H_y = \frac{-j\omega\epsilon}{k_{c^2}}\frac{m\pi}{a}A\cos(\frac{m\pi x}{a})\sin(\frac{n\pi y}{b})e^{-\gamma z}$

(2.1)

Where a and b are the inside width (longest dimension) and height (shortest dimension), respectively, m and n are the number of half-wavelength variations of field in the "a" and "b" direction respectively, and γ is the propagation constant. Further explanation and derivation for these formulas can be found in references [1],[2] and [3].

In order to understand these properties, the explanation of two new concepts is required: Perfect Electric Wall (PEW) and Perfect Magnetic Wall (PMW) symmetries. The definition is pretty straightforward, a mode is said to have a PEW symmetry with respect to a certain plane if the electric field is perpendicular to that plane. Likewise, a mode is said to have a PMW symmetry with respect to a plane if the magnetic field is perpendicular to

that plane. Furthermore, due to fact that the former equations are described in terms of sines and cosines, the electric and magnetic fields will inherit their properties and be either symmetrical or anti-symmetrical functions related to these walls.

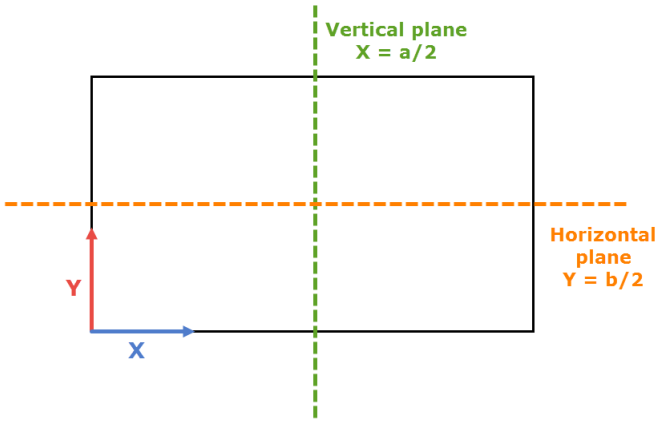

Figure 2.1: Rectangular waveguide cross section, reference system and symmetry planes.

Our interest is to determine which modes will have PEW or PMW symmetries specifically at the planes $y = \frac{b}{2}$ and $x = \frac{a}{2}$ as shown in the Figure 2.1. Therefore, our approach will be to see what happens to the fields in those planes using the equations in Formula 2.1 and making use of the similar structure in the field components. Finally, the Table 2.1 summarizes the process and conclusions.

$$\begin{aligned} E_x = H_y = 0 \begin{cases} y = \frac{b}{2} \rightarrow \sin(\frac{n\pi}{2}) & \Rightarrow \text{Horizontal PEW, } n = 0, 2, 4... \\ x = \frac{a}{2} \rightarrow \cos(\frac{m\pi}{2}) & \Rightarrow \text{Vertical PMW, } m = 1, 3, 5... \end{cases} \\ E_y = H_x = 0 \begin{cases} y = \frac{b}{2} \rightarrow \cos(\frac{n\pi}{2}) & \Rightarrow \text{Horizontal PMW, } n = 1, 3, 5... \\ x = \frac{a}{2} \rightarrow \sin(\frac{m\pi}{2}) & \Rightarrow \text{Vertical PEW, } m = 0, 2, 4... \end{cases} \end{aligned} \tag{2.2}$$

Rectangular TE	**Rectangular TM**	**Horizontal wall**	**Vertical wall**
$m = 0, 2, 4...$ $n = 0, 2, 4...$	$m = 2, 4, 6...$ $n = 2, 4, 6...$	PEW $\bar{E}$ antisymmetric $\bar{H}$ symmetric	PEW $\bar{E}$ antisymmetric $\bar{H}$ symmetric
$m = 0, 2, 4...$ $n = 1, 3, 5...$	$m = 2, 4, 6..$ $n = 1, 3, 5...$	PMW $\bar{E}$ symmetric $\bar{H}$ antisymmetric	PEW $\bar{E}$ antisymmetric $\bar{H}$ symmetric
$m = 1, 3, 5...$ $n = 0, 2, 4...$	$m = 1, 3, 5...$ $n = 2, 4, 6...$	PEW $\bar{E}$ antisymmetric $\bar{H}$ symmetric	PMW $\bar{E}$ symmetric $\bar{H}$ antisymmetric
$m = 1, 3, 5...$ $n = 1, 3, 5...$	$m = 1, 3, 5...$ $n = 1, 3, 5...$	PMW $\bar{E}$ symmetric $\bar{H}$ antisymmetric	PMW $\bar{E}$ symmetric $\bar{H}$ antisymmetric

Table 2.1: Table summarizing TE/TM modes symmetries.

In order to help the reader to check and understand the symmetries of some of the TE/TM modes, a group figures representing some of these modes is presented in Appendix A.

2.3 Waveguide Discontinuities: Higher-order mode generation

Waveguide structures are composite devices containing regions with different cross sections at certain planes; these surfaces are called discontinuities. Some discontinuities might be unavoidable results of mechanical defects in the waveguide manufacturing or undesired misalignment between two or more waveguides. However they might as well be deliberately introduced into the design in order to perform a specific electromagnetic function (stubs, filtering, impedance matching...).

In any event, electromagnetically speaking, these discontinuities impose certain boundary conditions that must be fulfilled by the electromagnetic field. Nonetheless, those new conditions usually imply the excitation of higher-order modes, in addition to the dominant mode, to be satisfied.

These higher-order modes might be then evanescent or propagating modes, depending on the working frequency with respect to the cutoff frequency of the mode (which itself depends on the dimensions of our waveguide). In our first case, the field of the mode will rapidly decay as it travels away from the source of excitation, whereas if the mode is propagating it will carry a portion of the incident power. It is up to the engineer to consider the generation of this modes and work with the attenuation levels if they were not intended to be in the design in the first place.

Following the former explanation and the conclusions in Table 2.1 the next group of figures will illustrate an example of the generation of higher-order modes due to different discontinuities. It is assumed that only the dominant TE_{10} mode is propagating in one side of the discontinuity and no modes are propagating in the other.

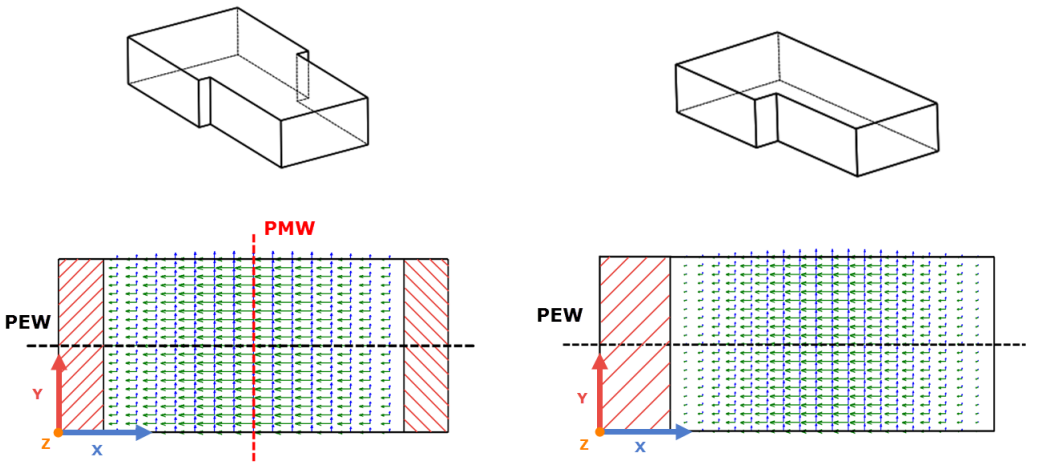

(a) Symmetrical H-plane discontinuity. (b) Asymmetrical H-plane discontinuity.

Figure 2.2: Symmetries of rectangular waveguide discontinuities. H-plane discontinuities.

Figures 2.2a and 2.2b show an H-plane step (change in width) in a rectangular waveguide. Our first figure holds symmetry both with respect to the

xz plane (PEW) and the yz plane (PMW), thus only the modes with such vertical symmetry will be excited, i.e, TE_{m0} modes with $m = 1, 3, 5....$ On the other hand, the second figure only holds symmetry with respect to the xz plane (PEW) and therefore all the modes TE_{m0} modes with $m = 1, 2, 3...$ will be excited. Note that there is no height variation in either figure, so all modes will preserve $n = 0$ (n is the height-variation) in this case.

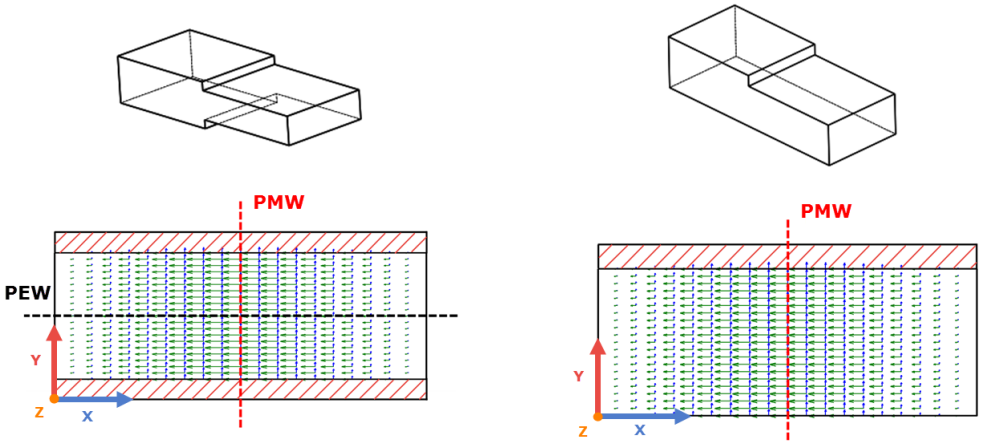

(a) Symmetrical E-plane discontinuity. (b) Asymmetrical E-plane discontinuity.

Figure 2.3: Symmetries of rectangular waveguide discontinuities. E-plane discontinuities.

Figures 2.3a and 2.3b show an E-plane step (change in height) in a rectangular waveguide. Note that this time there is no width variation in either figure, so all modes will preserve $m = 1$ and therefore we have to consider also TM modes, since none of the sub-indexes is zero. Once again our first figure holds both vertical and horizontal symmetry so TE_{1n}/TM_{1n} with $n = 2, 4, 6...$ will be excited. Similarly, the second figure only holds vertical symmetry so all the modes TE_{1n}/TM_{1n} with $n = 1, 2, 3...$ will be excited.

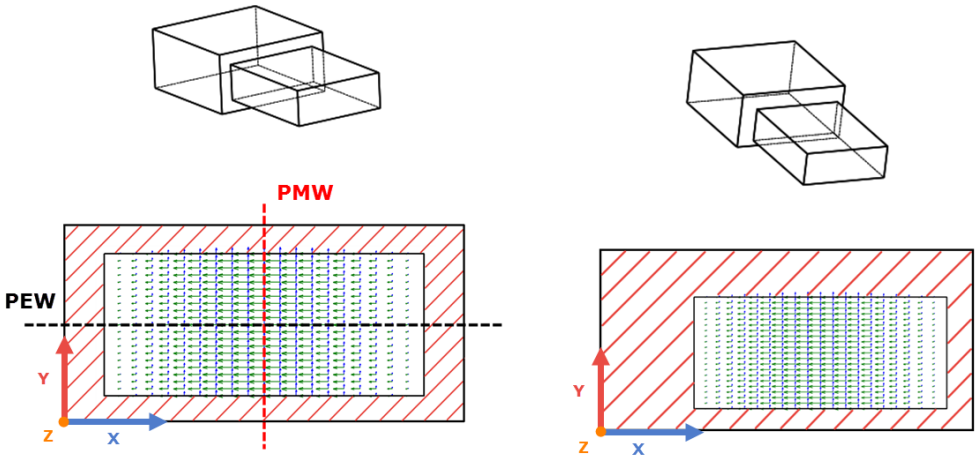

(a) General symmetrical discontinuity. (b) General asymmetrical discontinuity.

Figure 2.4: Symmetries of rectangular waveguide discontinuities. High and width variation.

Our last two figures show both width and height variation. Thus, as a combination of the two former cases in figure 2.4a, TE_{mn}/TM_{mn} with $m = 1, 3, 5...$ and $n = 2, 4, 6...$ will be excited. The discontinuity in figure 2.4b breaks all the symmetries, so all the TE/TM modes will be excited.

2.4 Scattering Parameters

When dealing with high-frequency networks, the measurement of equivalent voltages, currents and their related impedance and admittance may turn into a very hard task. Moreover, under non-TEM lines circumstances, these parameters might not be uniquely defined and they become somewhat of an abstraction.

In addition, in order to determine Y (admittance) or Z (impedance) matrices classic network theory requires open and short circuit conditions, which become very unstable when working on high-frequency devices and may often lead to undesired radiations or even the destruction of the device itself.

Scattering (S) parameters represent a much more useful way to describe microwave devices. Whereas impedance and admittance matrices relate the total voltages and currents at the ports, the scattering matrix relates the incident waves from the ports to those reflected from the ports. This configuration also leads to a stronger focus on power transferring in systems, leaving voltages and currents waves in the background.

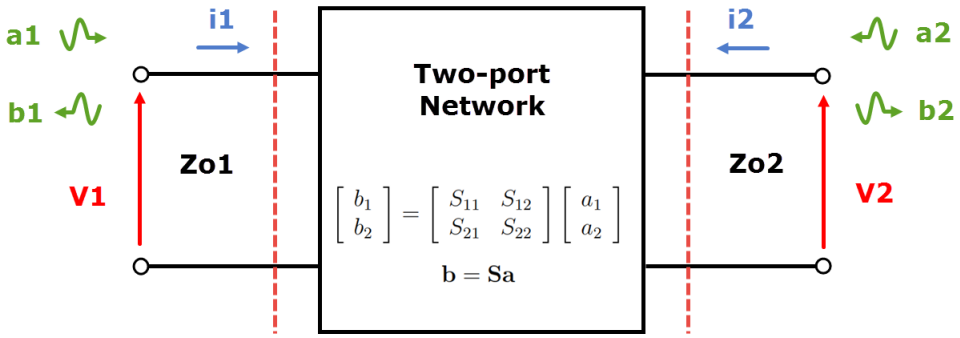

Figure 2.5: Parameters of a two port network

Therefore, in order to describe the S parameters we need to define a new set of waves for each port called *power waves*:

$$a_i = \frac{v_i + Z_{0i} i_i}{\sqrt{8 Z_{oi}}} \quad b_i = \frac{v_i - Z_{0i} i_i}{\sqrt{8 Z_{0i}}} \tag{2.3}$$

In equation 2.3 we are assuming that the reference impedance (Z_{0i}) is a real value. This is a decently realistic assumption since, in day to day designs, these impedances are specifically chosen to be the characteristic impedance

of the transmission lines acting as access to the net, which will be real for low loss scenarios.

On the other hand, it would be very useful to use "low-frequency" concepts such as impedance and admittance matrices, voltage or current, since a well established circuit theory already exists for them. We can formulate some of them making use of figure 2.5:

$$v_i = (a_i + b_i)\sqrt{2Z_{0i}} \quad i_i = (a_i - b_i)\sqrt{\frac{2}{Z_{0i}}} \tag{2.4}$$

Finally, we can define the S parameters depending on the power waves as the relation between an incident wave in port j and the reflected wave coming out in port i. The incident waves on all ports except the jth port are set to zero, which means that those ports should be terminated in matched loads to avoid reflections:

$$S_{ij} = \left.\frac{b_i}{a_j}\right|_{a_k=0,\ k\neq j} \tag{2.5}$$

The scattering matrix is then defined with all the different parameters:

$$\begin{bmatrix} b_1 \\ b_2 \end{bmatrix} = \begin{bmatrix} S_{11} & S_{12} \\ S_{21} & S_{22} \end{bmatrix} \begin{bmatrix} a_1 \\ a_2 \end{bmatrix} \qquad \mathbf{b} = \mathbf{S}\mathbf{a} \tag{2.6}$$

Thus, this matrix setting implies that, in this case, S_{11} and S_{22} are the reflection coefficients whilst S_{12} and S_{21} are the transmission coefficients. Often we refer to these coefficients through a couple of more common names: return and insertion losses, usually in decibels.

$$\begin{aligned} L_I &= -20\log(|S_{mn}|)\ \text{dB},\ m \neq n \\ L_R &= -20\log(|S_{mm}|)\ \text{dB} \end{aligned} \tag{2.7}$$

To end this section we will briefly mention some basic properties of the

scattering matrix such as reciprocity, symmetry and scattering matrix in loss-less networks.

We talk about reciprocal networks when the scattering matrix holds that $S_{ij} = S_{ji}$. The idea behind this property is that, given a pair of ports, the excitation and the outcome will be the same regardless of which port holds the excitation.

The symmetry depends on the physical geometry of the network and respect to which planes it holds symmetry with. In the simple case of a two-port network it will imply that $S_{11} = S_{22}$.

And for a loss-less network the incident power must be equal to transmitted plus the reflected power, again in the simplest case of a two-port network, this translates into $|S_{21}|^2 + |S_{11}|^2 = 1$ and $|S_{12}|^2 + |S_{22}|^2 = 1$.

Of course, all these concepts and definitions can also be applied to multiport networks. If that were the case, the scattering matrix would look something of the form:

$$\begin{bmatrix} b_1 \\ b_2 \\ b_3 \\ \vdots \\ b_M \end{bmatrix} = \begin{bmatrix} S_{11} & S_{12} & S_{13} & \cdots & S_{1M} \\ S_{21} & S_{22} & S_{23} & \cdots & S_{2M} \\ S_{31} & S_{32} & S_{33} & \cdots & S_{3M} \\ \vdots & \vdots & \vdots & & \vdots \\ S_{M1} & S_{M2} & S_{M3} & \cdots & S_{MM} \end{bmatrix} \begin{bmatrix} a_1 \\ a_2 \\ a_3 \\ \vdots \\ a_{M;} \end{bmatrix} \tag{2.8}$$

It is important to highlight the difference between a physical port and an electrical port. This means, if one physical port has more than one mode (either propagating or evanescent mode) present within the waveguide each of them is represented by one electrical port, and therefore this will increase the number of elements in the S matrix with respect to the number of physical ports. When the S matrix includes evanescent modes it is called Generalized Scattering Matrix, and all the former concepts and properties might not apply in this case.

2.5 Polarization

During the elaboration of this project the term "orthogonal polarization" is frequently adopted to explain OMT theory; therefore, as a brief reminder to the reader, the condition of linear and circular polarization will be explained in this section.

The concept of polarization is directly related to the time variation of the electromagnetic field vectors at any point of the space, generally determined by the orientation of them. Considering the z coordinate as the propagation direction in the positive direction, the electric field of a plane wave can be written as:

$$\overrightarrow{E} = (E_x\hat{x} + E_y\hat{y})e^{-\gamma z}$$

where γ is the propagating constant and E_x and E_y are the orthogonal components aligned with the x and y axes, respectively. A number of options now arise. If the field does not exhibit a vertical component, i.e., $E_y = 0$ then the polarization will be referred as horizontal. Likewise, a vanishing horizontal field component, i.e., $E_x = 0$ yields a vertical polarization. If E_x and E_y are both real or pure imaginary, nonzero components that are in phase, the plane wave is still linearly polarized with and orientation in the xy plane such as:

$$\phi = \tan^{-1}\left(\frac{|E_y|}{|E_x|}\right)$$

Both horizontal and vertical polarizations can be transmitted independently owing to *decoupling by orthogonality*. Note that this is still applicable in the last case mentioned above by using a new rectangular coordinate system, x' and y', with and angular offset of ϕ. With this new reference, as shown in figure 2.6, $E_{x'}$ represents the x' (horizontal) polarization whereas $E_{y'}$ fields are transmitted by the y' (vertical) polarization.

Unlike in the case of linear polarization, where the orientation of the $\overrightarrow{E}$ field is constant within the xy plane, the $\overrightarrow{E}$ field of a circularly polarized wave propagates along a circularly helix in the z direction. Mathematically it is

described by two linear orthogonal field components with the same magnitude but a *phase difference* of $\pm\frac{\pi}{2}$. If any of these three conditions is not satisfied (either orthogonality, equal magnitude or a phase difference of $\pm\frac{\pi}{2}$ between them) the wave is referred as elliptically polarized, which might heavily affect the discrimination of the two different signals within a dual polarized system.

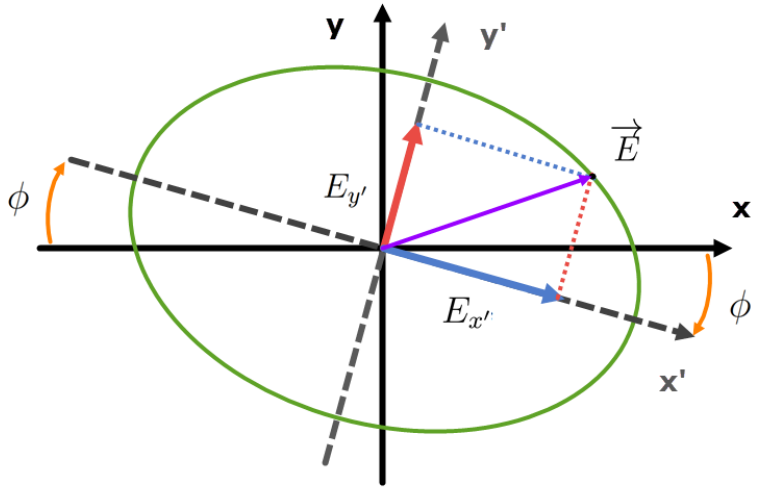

Figure 2.6: Coordinate system for dual linear polarization.

The former conditions determine a circular propagating wave with the form

$$\vec{E} = E_0(\hat{x} \pm j\hat{y})e^{-\gamma z} \tag{2.9}$$

$$\text{Time Domain} \Rightarrow \vec{\mathcal{E}}(z,t) = E_0[\hat{x}\cos(\omega t - \gamma z) \pm \hat{y}\cos(\omega t - \frac{\pi}{2} - \gamma z)]$$

Note that the $\pm$ sign refers to either *right-hand circularly polarized* (RHCP, $-$ sign) or *left-hand circularly polarized* (LHCP, $+$ sign). This equation shows that the electric field vector changes either with time or with distance along the z axis. For instance, if we pick a fixed position say $z = 0$, we can see that

electric field vector rotates clockwise or counterclockwise from the x axis. The resulting angle from the x axis would be then

$$\phi = \tan^{-1}\left(\frac{\sin(\omega t)}{\cos(\omega t)}\right) = \omega t$$

which shows that the field vector rotates at the uniform angular velocity ω.

2.6 Conclusions

Basic concepts and definitions have been explained during this chapter, thus giving us some insight on the modes and symmetries of a rectangular waveguide. This background will be essential to understand the upcoming sections.

Although a special focus has been laid upon the rectangular waveguide technology (since it is the technology that will be used during the design of our project), a very similar analysis of modes and symmetries can be carried out for circular waveguides. A breakdown of this process is not going to be done in this document; however, this technology will be mentioned in next chapters since the conclusions have analogous results to the ones presented.

Chapter 3

OMT Introduction

3.1 Motivation

The inclusion of this chapter into the document is not only motivated by the need for introducing this technology to the reader, but also by the unsatisfactory treatment given to this field by the literature. Despite of the usefulness of these devices during the last years, the mentions and publications concerning OMTs usually present very specific designs, built for very precise applications.

Bøifot published a couple of classifications during the 90's, however the technique was in sort of an early state by then, and several configurations have been proposed after his papers. In [4] they classified OMTs into "simple narrowband" and those based on Bøifot or Turnstile junctions. Later on, a wider classification was published in [5], this time sorting them into five main groups depending if they were based on waveguide-to-waveguide transitions or waveguide-to-coaxial transitions.

Finally, Uher along with other engineers published [6]. Again, although the literature about OMTs in particular is very limited (even in that book), it is the latest and more modern classification of OMTs there is so far and, in fact, the concepts and teachings explained in it had a considerable role in this document. Inside, they classified the OMTs in three main groups: narrowband, wideband and multiband. Additionally it is a broad source of figures and plots of different structures, which might be referenced in the following sections.

3.2 Functions and theory of OMTs

Ortho-Mode Transducers (OMTs) are used in numerous telecommunication systems in the modern world, frequently found in environments regarding satellite communications or radio astronomy. After all, due to the growing bandwidth demand in telecommunications, an efficient use of the available spectrum has grown more and more relevant, and that is precisely the strength of OMTs. This device basically doubles the number of channels that can be served at a certain frequency, since two different signals can be transmitted or received in the same frequency range as long as they are orthogonally polarized. Of course, depending on the application the OMT is designed for, you might focus on improving some features rather than others: return losses, bandwidth, isolation... and thus, prioritizing certain configuration over the rest.

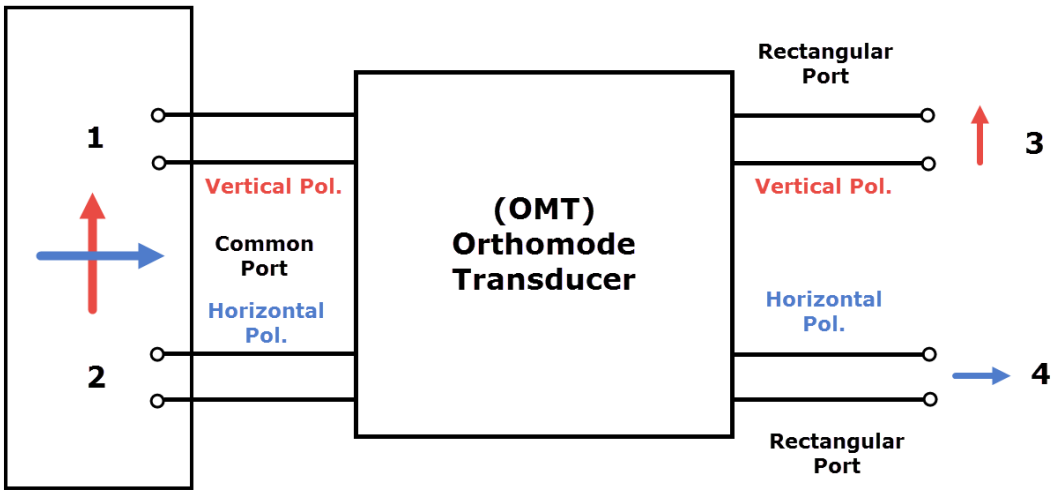

Figure 3.1: Block diagram of an Ortho-Mode Transducer.

OMTs are passive microwave devices with four electrical ports, although it presents only three physical ports. This results from the fact that the *com-*

mon port (usually with square or circular cross section) provides two electrical ports, designed to the orthogonally independent fundamental modes, whereas the two remaining ports serve their respective fundamental mode only. Their task is to act as polarization discriminators. In receivers, they separate the incoming dual-polarized signal through the common port into two single signals at the output ports. Similarly, they are used the other way around in transmitters, combining the two signals fed at the *single-mode ports* into the common port while maintaining them uncoupled due to the orthogonal polarization.

Figure 3.1 shows the port distribution we mentioned above. Following this diagram, from now on we will refer to port 1 as the vertical polarization in the common port and port 2 for the horizontal polarization. Likewise, port 3 will be the single-mode port for the vertical polarization and port 4 for the horizontal polarization.

As many other high-frequency components, OMTs can be completely characterized by its scattering matrix (briefly explained in Section 2.4). An ideal OMT has an S-matrix such as:

$$\mathbf{S} = \begin{bmatrix} 0 & 0 & e^{j\phi_1} & 0 \\ 0 & 0 & 0 & e^{j\phi_2} \\ e^{j\phi_1} & 0 & 0 & 0 \\ 0 & e^{j\phi_2} & 0 & 0 \end{bmatrix} \tag{3.1}$$

where, as it can be seen, all the power is transferred from port 1 to 3 and from port 2 to 4 (since it is a reciprocal device). This implies that, ideally, no power would be transferred from port 1 to 4 or from port 2 to 3.

However, when building a real OMT there are some impairments on the match and isolation of the design as a result of the higher-order mode excitation. It is up to the designer to reduce the effect of these undesired higher-order modes by the correct use and placement of the required discontinuities, junctions or matching elements. Here is where the concepts and information described in Chapter 2 proves valuable.

In the next sections we will talk about different configurations of OMTs, making a special focus on narrowband OMT, since it applies directly to our design. Nonetheless we will briefly mention some techniques regarding wideband OMTs, due to their importance in some of the technology nowadays.

3.3 Narrowband OMTs

This kind of OMT is widely used in commercial communication systems due to its simplicity and low fabrication expenses. They provide a high performance within a narrow frequency band, generally around 10% of *fractional bandwidth* (FBW). In the best case scenario, their FBW is limited to a maximum of 34.3% for those using a square waveguide as common port, and to a maximum of 26.6% for those using a circular waveguide common port instead. This results from the fact that these structures hold no more than one symmetry plane and the cutoff frequency of the higher-modes (TE_{11}/TM_{11} for square waveguide and TM_{01} for circular waveguide) is fairly close to the operating frequency. Generally these OMTs exhibit waveguide interface ports, although few designs may require from coaxial ports, referring to this adaptation as *hybrid OMTs*. The following subsections will analyze different configurations of narrowband OMTs, presenting some figures for further understanding.

3.3.1 Taper/Branching OMT

This design is based on a longitudinal taper section proving a symmetrical or asymmetrical transition of the common square or circular waveguide to the standard waveguide interface of one fundamental mode, normally referred as *axial or vertical port*. A waveguide branching is placed perpendicularly to the longitudinal axis, with its broad dimension aligned to the taper section. The location of this branching is of decisive importance for a good performance of the device, specially for the horizontal (TE_{01}in rectangular waveguide) mode. Figure 3.2 illustrates the principal designs for this OMT type.

The analysis of the modes behavior in a rectangular waveguide is described as follows: As the dominant (TE_{10}) mode travels through the waveguide from the common port, only modes with vertical PMW symmetry will excite (see reference in Section 2.3). However, these modes are under cutoff regarding the branching waveguide so they can only be reflected back to the common port or coupled to dominant mode towards the axial port.

This same process occurs with the orthogonal dominant mode (TE_{01}) although the vertical symmetry now is regarding PEW (see reference in Section 2.3). This time, this symmetry excites the TE_{10} fundamental mode of the

branching waveguide, and thus, there is power transfer between ports 2 and 4.

Different taper designs can be seen in Figure 3.2, using structures ranging from continuous contour function along the longitudinal axis to stepped waveguide transformers. In order to improve the matching properties regarding the branching port it is usual to one or more inductive iris as well.

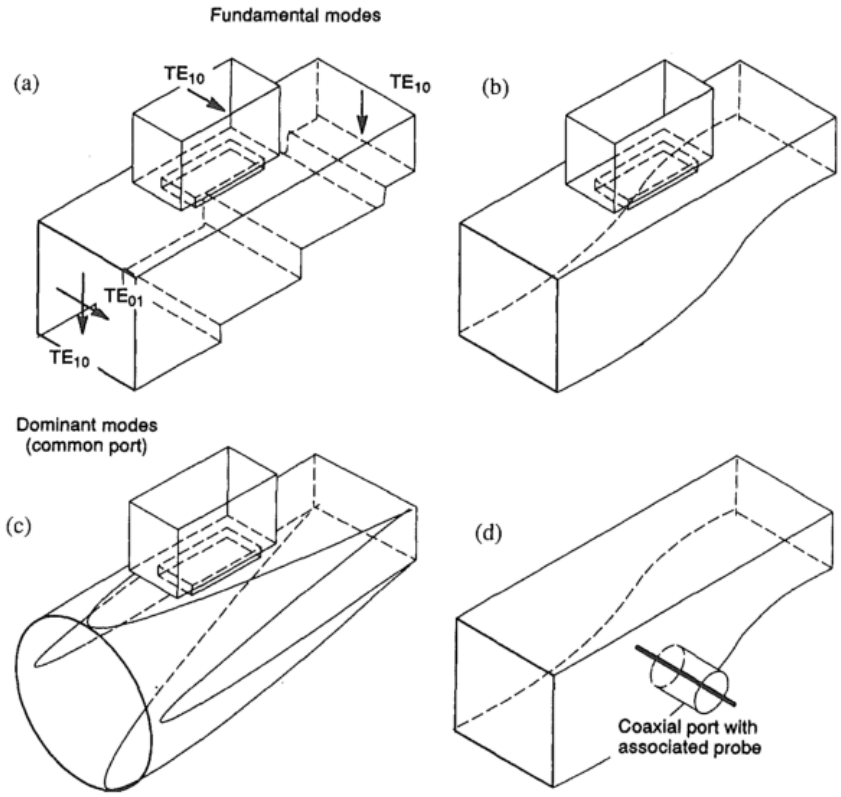

Figure 3.2: Narrowband OMT type 1. Taper/branching OMT designs. Illustration from [6], Chapter 3; J.Uher, J. Bornemann and U. Rosenberg, 1993.

3.3.2 Septum/Branching OMT

This OMT type makes use of a uniform cross-section of the common port waveguide. The septum section should be placed right before or partially overlapped by the branching waveguide, with the broad dimensions of this region generally in line with the longitudinal axis of the common waveguide, as illustrated in Figure. This section is seen as it has been divided into two regions of half height in terms of TE_{01} and thus it becomes evanescent, begin reflected and coupled to the branching port in a similar way to the former taper/branching type.

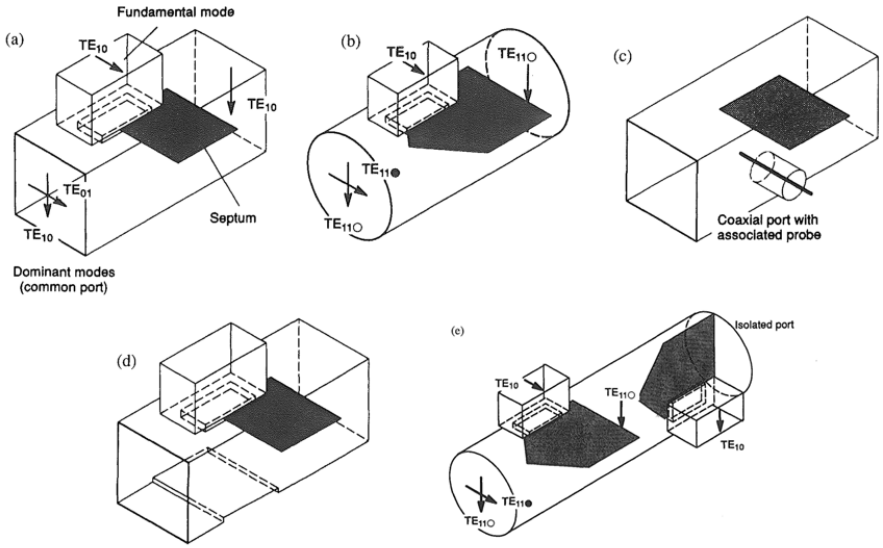

Figure 3.3: Narrowband OMT type 2. Septum/branching OMT designs. Illustration from [6], Chapter 3; J.Uher, J. Bornemann and U. Rosenberg, 1993.

Other improvements in terms of matching for this OMT type might include specific-shaped septum (Figure (b) of 3.3) and a capacitive discontinuity at the wall facing the branching waveguide (Figure (d) of 3.3) . A standard rectangular waveguide interface for the axial port can be obtained by the application of the techniques used in the former OMT type, such as a

standard taper or a stepped waveguide transformer; nevertheless, the same effect can be achieved by using the septum section twice (Figure (e) of 3.3) .

3.3.3 Acute Angle or Longitudinal Ortho-Mode Branching

As the reader may have already guessed by the name, this OMT type is characterized by its branching region, where both single-mode ports ramify under and *acute angle* from the longitudinal axis of the common waveguide. If the whole structure presents nearly the same cross-section, some septum might be needed in order to make the undesired mode evanescent in the respective port.

Figure 3.4 shows different configurations for this OMT type. The main drawback of these designs results from the complexity of the branching region, which often causes matching or isolation difficulties due to excitation of higher-order modes. Additionally, they generally have a high manufacturing expense.

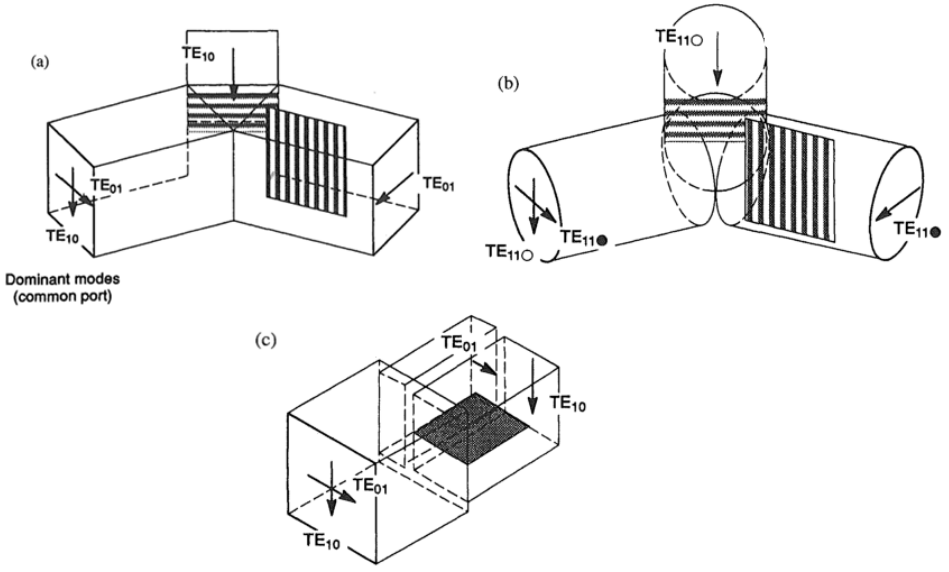

Figure 3.4: Narrowband OMT type 3. Acute angle OMT branching. Illustration from [6], Chapter 3; J.Uher, J. Bornemann and U. Rosenberg, 1993.

3.3.4 Short Circuited Common Waveguide

This last OMT type represents the simplest design. In this configuration the structure presents two rectangular branching waveguides, both situated at perpendicular side walls of the common waveguide and placed at fixed distance from the short circuit plane, determined by

$$l_{1,2} = \frac{\lambda_{g1,2}}{4}$$

where $\lambda_{g1,2}$ represents the common waveguide wavelength of the respective fundamental mode at the center frequency of the operating band. Note that in the case that the common waveguide was not square, $\lambda_{g1} \neq \lambda_{g2}$ and thus the branching ports would be placed at different locations.

The essential drawback for this OMT type is the excitation of higher-order modes within the asymmetric branching region, which frequently leads to direct coupling between the ports. Moreover, adequate matching and isolation properties can hardly be achieved by this design for a bandwidth of 10%.

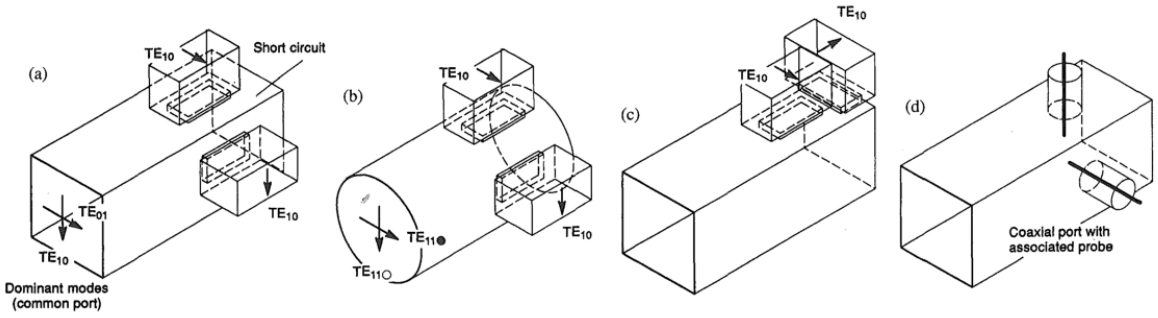

Figure 3.5: Narrowband OMT type 4. Short circuited common waveguide. Illustration from [6], Chapter 3; J.Uher, J. Bornemann and U. Rosenberg, 1993.

3.4 Wideband OMTs

This type of OMT is also referred as *Broadband OMT*, and they can get to cover up to a 90% FBW. To be able to serve this purpose it is necessary that they include an in-nature broadband structure into the device. An in-depth look into this selection of OMTs is out of the scope of this project; nevertheless, this section will hover over the different configurations and emphasize the design considerations that allow these devices to have such a broad bandwidth and even provide a high performance over more than 60% FBW. As the reader will see over the next paragraphs, their symmetry properties is the key to an appropriate treatment of the undesired higher-order modes and, in result, an increasing single-mode bandwidth.

3.4.1 Bøifot junction or Distinct dual Junction Type

The major building block of this design is the symmetric 5-port branching, shown in Figure 3.6. The dual-polarized signal at the common port is split into four single signals. The longitudinal signal travels through the first dual junction to the ports P_1 and P_2, which have standard waveguide cross-section (i.e. same width and half height of the common port). The second dual junction, providing ports P_3 and P_4, is produced by a pair of E-plane T-junctions for the corresponding fundamental modes that occupy the respective opposite side walls of the branching section. It is common to add one or two metallic posts at both side arms, to help improve matching at some frequencies. Additionally, a thin septum is necessary in order to achieve a good performance, as it favors wave splitting and overall matching in a similar way to former configurations.

Each of these four signals carry half the power of the polarized wave (vertical or horizontal, respectively), if the junction is properly designed. The design of this septum is the main drawback of this architecture because of its complexity. Manufacturing these septum and posts at high frequencies (i.e., hundreds of GHz) is quite critical, as they become too small and mechanically unstable.

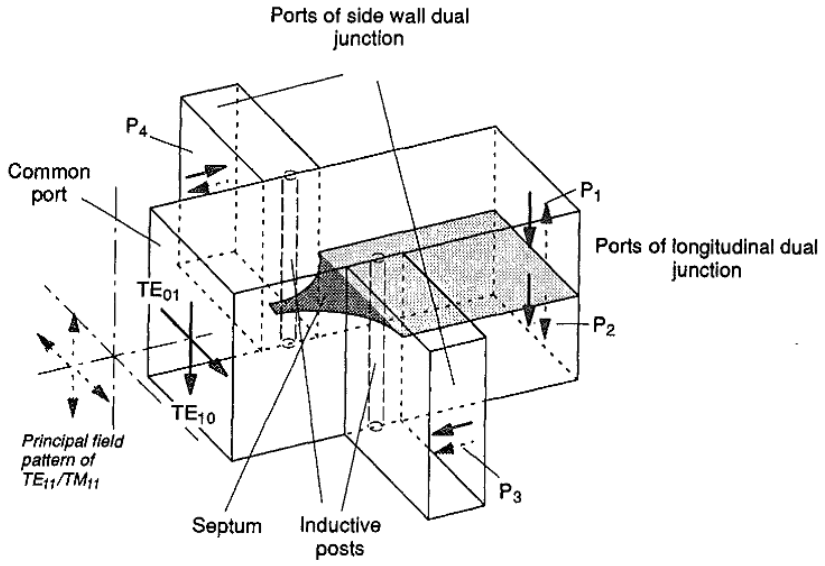

Figure 3.6: Bøifot junction OMT design. Illustration from [5]

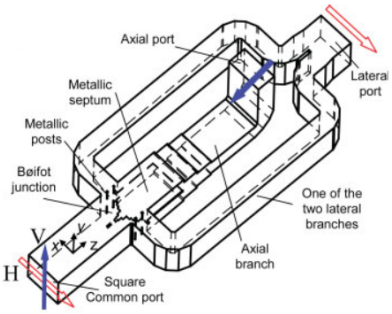

(a) Bøifot junction. E-plane bends recombination. Illustration from [7].

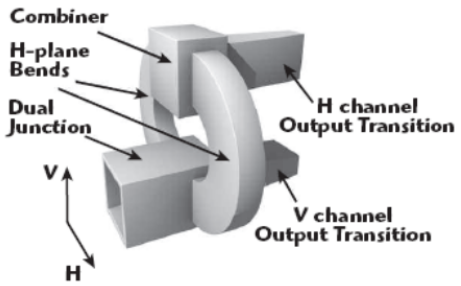

(b) Bøifot junction. E-plane bends recombination. Illustration from [8].

Figure 3.7: Reflection coefficients of Vertical mode.

Due to this 5-port "half power" configuration a recombination of the respective ports is required. Since signals in ports P_1 and P_2 are always combined after the septum, these ports are usually treated as a unique through-port. However, it is not that simple in terms of the horizontal mode signals. Generally this recombination is made by means of E/H-plane bends.

E-plane bends have the advantage of holding full symmetry over two planes and therefore allowing to avoid the excitation of the first undesired higher-order modes, increasing the single-mode bandwidth (e.g. Figure 3.7a). On the other hand, *H*-plane bends provide and overall reduced size of the device at the cost of holding only one plane symmetry (e.g. Figure 3.7b).

Thanks to the twofold symmetry of the Bøifot junction, the first higher-order modes that are excited in this structure are the $TE_{12}/TM_{12}/TE_{21}/TM_{21}$, which represents a 76.4% theoretical FBW for the OMTs based on this junction.

3.4.2 Turnstile junction

Similarly to the Bøifot junction, the Turnstile Junction is also a 5-port structure, composed of a common port and four single-mode ports. It also separates each polarization into two halves of equal power; nonetheless, the main difference with respect to the Bøifot junction lies in its identical behavior for both polarizations, which provides *fourfold symmetry*. As a matter of fact, no additional structures are required to achieve a high performance over a wind band, saving us from using septum or posts. It should noticed though, that a small obstacle (sort of a pyramidal object) in the wall facing the common guide helps splitting the waves and matching for broadband performance.

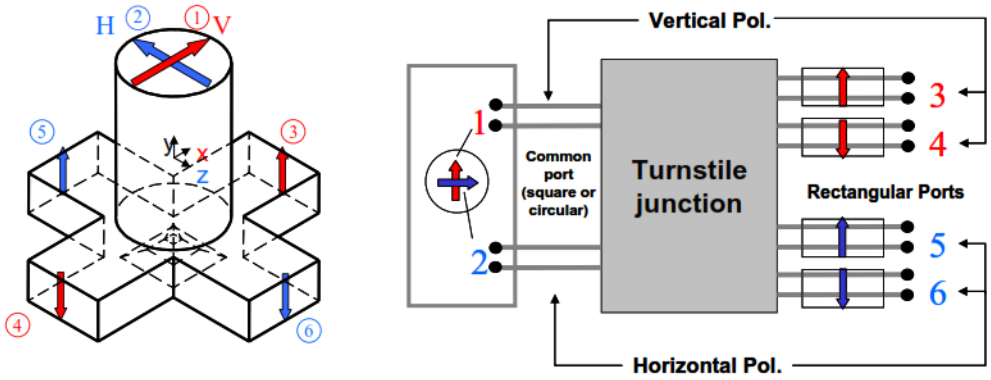

Figure 3.8: Physical and electric diagram of the Turnstile junction. Illustration from [8].

Figure 3.8 illustrates the operation principle. However, designs making use of this junction tend to be actually pretty complex and no further elaboration will be made in this document. Figure 3.9 shows example of actual designs using this junction, with some recombination techniques already added.

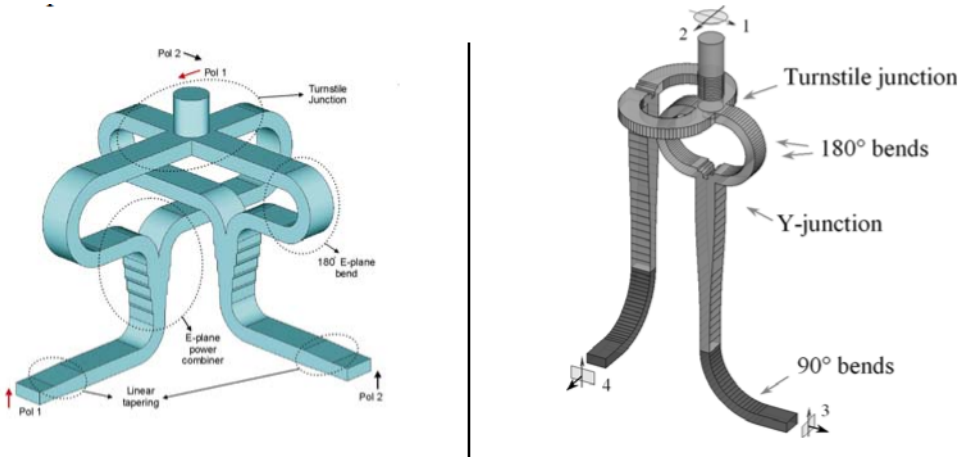

Figure 3.9: Recombination techniques in the Turnstile junction. Illustration from [8].

3.4.3 Finline OMT

As the name of this OMT type suggest, this design basically consists of a square or circular waveguide with two diametrically opposite thin tapered metallic fins inside. The operation principle is fairly similar to the Septum/branching (section 3.3.2) or the Bøifot junction (section 3.4.1) based ones. The main difference with respect to septum/branching design is that, in this case, these fins confine the energy of the horizontal mode to the gap between them and direct it from the waveguide to the port by a bend, which normally is of 90^{o}.

In terms of relations between ports and higher-mode generation, the analysis is analogous to those previously explained in the narrowband OMT section.

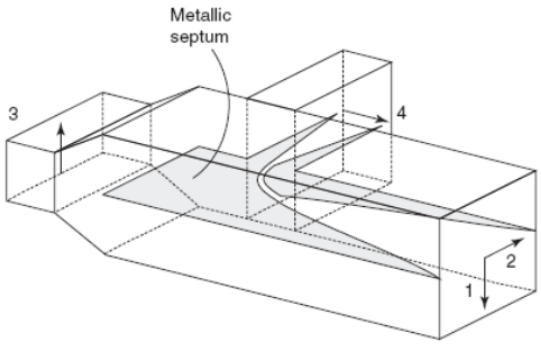

Figure 3.10: Finline OMT design. Illustration from [8].

3.4.4 Double-Ridged and Quad-Ridged OMT

Both this configurations are slight variations of the finline OMT. In the first case the OMT concentrates one of the polarizations between to ridges in the center of the square waveguide, removing then its power by a coaxial line. Meanwhile the other polarization is not affected by this ridges, traveling directly through a rectangular transition after which its power is extracted by a coaxial line as well. On the other hand, in the Quad-Ridged configuration two orthogonal pairs of finlines concentrate both fundamental modes in the center of the guide. Unfortunately, further elaboration in the operation process goes out of the scope of this document, as these structures deal with rather complex issues of matching with the coaxial probes.

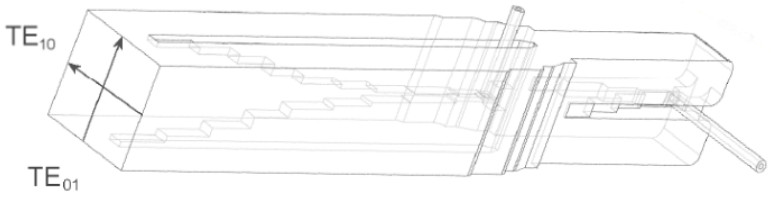

Figure 3.11: Double-Ridged OMT design. Illustration from [8].

3.5 Polarizers

As the reader might have already noted after this brief introduction, all these OMT designs operate over linearly polarized waves. If circular polarization is required, a proper polarizer should be placed between the antenna horn and the OMT to transform the polarizations, which is actually very common in nowadays reception systems. The design of these polarizers is out of the scope of this project, although its performance and configuration can be found in [6].

Additionally, there are structures that include this polarizer into the design and thus reducing the overall size and weight. As a disadvantage though, this configuration doesn't offer the same level of performance as using polarizer-OMT separately.

3.6 Our device

The purpose of this section is to link our device with one or more types of the different OMT that have been analyzed, as well as specifying the ports and modes numbers. Hopefully, this will lead to a clear terminology to work with in the last chapter of the document, where each step of the design is elaborated.

As said before in this chapter, we will design a narrowband ortho-mode transducer, making use of the taper/branching and septum/branching configurations to achieve our design goals, which will be further explained in Chapter 5.

Adjusting a little bit how the scattering parameters have been presented in section 3.2 and on behalf of the simulations that later on will take place, we will define the S-parameters and matrix terminology as

$$S_{port(mode)port(mode)}$$

$$\mathbf{S} = \begin{bmatrix} S_{1(1)1(1)} & S_{1(1)1(2)} & S_{1(1)2(1)} & S_{1(1)3(1)} \\ S_{1(2)1(1)} & S_{1(2)1(2)} & S_{1(2)2(1)} & S_{1(2)3(1)} \\ S_{2(1)1(1)} & S_{2(1)1(2)} & S_{2(1)2(1)} & S_{2(1)3(1)} \\ S_{3(1)1(1)} & S_{3(1)1(2)} & S_{3(1)2(1)} & S_{3(1)3(1)} \end{bmatrix}$$

where the first and third subscript refer to the physical port of the structure, and the second and fourth (those between parenthesis) refer to the mode in that physical port.

Therefore, and since the OMT will be designed in rectangular waveguide technology, further clarification can be made as follows: we will refer to the first physical port as the common square waveguide port, in which the TE_{10} mode and TE_{01} mode are the number 1 and 2 respectively. Similarly, the axial and branching port will be referred as port 2 and 3 respectively, in which only the fundamental mode is excited.

3.7 Conclusions

An attempt to summarize most of the OMT types has been done through this chapter, recollecting the scattered contributions made in technical literature during the last years. Hopefully, this process has granted the reader with a bigger picture of all the various designs available for OMTs. Essentially they have been classified into narrowband and broadband structures, this resulting from the way that higher-order modes are excited within them.

Also a relation between this classification and our design has been pointed out, which along with chapters 1 to 3, has prepared the reader to comprehend the last part of this document as the specific design of our device is addressed.

Chapter 4

Analysis and Design: Tools and Techniques

4.1 Motivation

The aim of this brief chapter is to describe the tools and programs that have been used in this project to analyze and design the different structures that compose the whole OMT. Unfortunately, due to the lack of analytical tools for direct design of these structures, many steps had to be designed by numerical optimization. However, this process has been always driven by the knowledge and comprehension of the structure to design. The two main programs used to carry out this project have been CST Microwave Studio (Computer Simulation Technology) and MATLAB.

4.2 CST Microwave Studio: Simulation and Optimization

CST Microwave Studio has been the full-wave analysis tool used in this project.

Full wave analysis is the process by which we solve the complete set of Maxwell's equations for a certain structure without any simplifying assumptions. This technique is often used to analyze electrically-large structures, i.e. when its physical size is much larger compared to the operating wavelength.

Specifically, CST is based on the FIT (Finite Integration Technique).

This is a spacial discretization scheme to numerically address the full-wave analysis of complex 3-D structures in time and frequency domain. This discretization of the problem creates a mesh of the geometry under analysis which, depending on its refinement, will deliver more or less accurate results. The more dense the mesh used, the more precise the results given; but also, the longer the computation time spent in the process. Generally an adaptive mesh technique is used, which means that the mesh is progressively more refined in the zones where the field has more variations. One of the many highlights of this technique is that, in time domain, the numerical effort of FIT increases more slowly with the problem size than other employed methods.

When it comes to optimization, *Nelder-Mead Simplex* has been the algorithm used during this project. This numerical method is commonly applied to nonlinear optimization problems for which derivatives may not be found, since it only requires function evaluations. It is not very efficient in terms of the number of evaluations it requires but it may frequently be the best method for a problem whose computational burden is relatively small. Further elaboration about this method can be found in [9].

4.3 MATLAB

As a secondary software, MATLAB has been used as the calculation tool for many steps during the design.

As a matter of fact, given the fairly deep theoretical background about TE/TM modes in waveguides required for this work, a simulator for computing and plotting these electromagnetic fields inside waveguides (of rectangular or circular cross section) was developed. This small preliminary project was initially approached as a warm-up activity to get a first idea of what is happening in the technology under study; however, in the end it was used to understand and illustrate several sections in Chapter 2.

Additionally, more MATLAB code has been developed to carry out other parts of the designing process, as well as being used as primary representing tool for the results obtained from the CST MS simulations.

4.4 Design process

The design process does not follow a cycle pattern right away, but rather at the end of the development. This results from the need to add different structures to the device depending on which signal path adaptation we look to improve. The designing process can be broke down in following steps:

- Specifications: Define the values of the transmission and reflection coefficients desired for our device.
- Ports and bandwidth: Choose the dimensions of our ports along with the simulation and optimization bandwidth.
- First adaptation of both ports: Addition of the necessary structures to achieve a minimum adaptation of both signal paths.
- Optimization: Cycle in which a commitment or middle point between the adaptation of both modes has to be found. This will require from small variations of the different components building the structure.

Figure 4.1tries to illustrate the different steps in a flowchart.

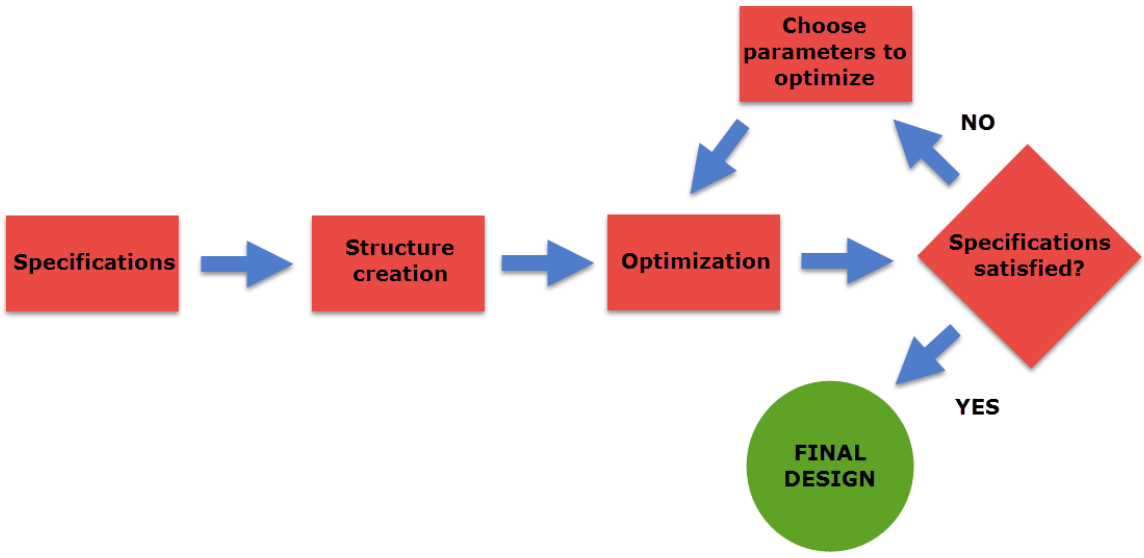

Figure 4.1: Design process flowchart.

4.5 Conclusions

The analysis and design tools used in this project have been described along with the use given to them in this work. Also, a summary of the designing process has been presented.

Finally, after a reminder of the theoretical background in waveguide electromagnetism in chapter 2, an introduction to OMTs in chapter 3 and the tools description in this chapter; the reader is fully ready to dive into the design of our Ortho-Mode Transducer.

Chapter 5

OMT Design

5.1 Motivation

Finally as the last step of this project, we will address the design of a narrowband OMT, working in the within the X-band frequencies. In order to reach the final design, we will need to start calculating the dimensions of our device's ports, since they are directly related with the operating frequency. Later on, other structures will be added to the design and, using the knowledge acquired about them in section 3.3, a cycle of optimizations will be carried out until the final design is achieved, which must satisfy the specifications set earlier in the document.

5.2 Dimensions, simulation bandwidth and modes excitation

Our first step to design our Ortho-Mode Transducer will be to choose the port dimensions. These dimensions will define and the limits of our device since the cutoff frequency of our modes depend on them. In order to choose our lateral and axial ports we will use the WR waveguide designation system, a standard widely use around the globe for rectangular waveguides.

Since our OMT will be design to work in X-band frequencies, we will use the standard WR-90 as the dimensions for our output ports, i.e., 22.86×10.16 mm . As input port we will use a square waveguide, that way both TE_{10} and TE_{01} will have the same cutoff frequency, since they are degenerate

modes. Its dimensions will be 20×20 mm.

WR DESIGNATION	WG EQUIVALENT	STANDARD FREQ RANGE GHZ	INSIDE DIMENSIONS (INCHES)
WR340	WG9A	2.20 - 3.30	3.400 x 1.700
WR284	WG10	2.60 - 3.95	2.840 x 1.340
WR229	WG11A	3.30 - 4.90	2.290 x 1.150
WR187	WG12	3.95 - 5.85	1.872 x 0.872
WR159	WG13	4.90 - 7.05	1.590 x 0.795
WR137	WG14	5.85 - 8.20	1.372 x 0.622
WR112	WG15	7.05 - 10.00	1.122 x 0.497
WR90	WG16	8.2 - 12.4	0.900 x 0.400
WR75	WG17	10.0 - 15.0	0.750 x 0.375
WR62	WG18	12.4 - 18.0	0.622 x 0.311
WR51	WG19	15.0 - 22.0	0.510 x 0.255
WR42	WG20	18.0 - 26.5	0.420 x 0.170
WR28	WG22	26.5 - 40.0	0.280 x 0.140
WR22	WG23	33 - 50	0.224 x 0.112
WR19	WG24	40 - 60	0.188 x 0.094
WR15	WG25	50 - 75	0.148 x 0.074
WR12	WG26	60 - 90	0.122 x 0.061

Figure 5.1: WR designation system.

Now, we will analyze the cutoff frequency of the dominant modes as well as some higher-order modes in our ports and, with that information, a simulation and optimization bandwidth will be set. As a reminder to the reader, cutoff frequency in a rectangular waveguide (square waveguide is just a particular case of rectangular waveguide) is defined as follows:

$$f_{cutoff} = \frac{\sqrt{\left(\frac{\pi m}{a}\right)^2 + \left(\frac{\pi n}{b}\right)^2}}{2\pi\sqrt{\mu_0 \epsilon_r \epsilon_o}} \tag{5.1}$$

The derivation of this formula is pretty straight forward due the nature of k_c, the cutoff wave number. However, further explanation on this matter can be found in [1]. Introducing our initial parameters in equation 5.1 we will get following values:

Rectangular Waveguide		Square Waveguide	
TE_{10}	$f_c = 6.557$ GHz	TE_{10}	$f_c = 7.495$ GHz
TE_{01}	$f_c = 14.750$ GHz	TE_{01}	$f_c = 7.495$ GHz
TE_{11}/TM_{11}	$f_c = 16.150$ GHz	TE_{11}/TM_{11}	$f_c = 10.600$ GHz
TE_{20}	$f_c = 13.110$ GHz	TE_{20}	$f_c = 14.990$ GHz

Table 5.1: Cutoff frequency of rectangular (22.86×10.16 mm) and square (20×20 mm) waveguide.

Using these results we will set our lowest simulation bandwidth value to 0.1 GHz above the cutoff frequency of the dominant mode (TE_{10}) of the input port, i.e., 7.6 GHz. Likewise, we set the highest simulation bandwidth value to 0.1 GHz below the cutoff frequency of the first higher-order mode (TE_{11}) of the square port, i.e., 10.5 GHz.

This will leave us with a simulation bandwidth such as:

$$\Delta_{sim} = 2.9 \text{ GHz} \Rightarrow 7.6 \sim 10.5 \text{ GHz}$$

$$f_{center} = 9.05 \text{ GHz}$$

5.3 Design goals and optimization bandwidth

As explained before in sections 3.3 and 3.6, due to the configuration we are using for this OMT our goal is to achieve a high performance over a ~10% bandwidth. Therefore we set our optimization bandwidth as:

$$\Delta_{opt} \simeq 0.1 f_{center} \approx 1 \text{ GHz}$$

$$\Delta_{opt} \Rightarrow f_{inf} = 8.5 \text{ GHz} \; ; \; f_{sup} = 9.5 \text{ GHz}$$

As the reader may have already noticed with the approximations we have

carried out we will end up with a *Fractional Bandwidth* a little bit higher than 10%:

$$FBW = \frac{f_{sup} - f_{inf}}{f_{center}} \times 100 = 11.11\%$$

Finally, we will express the specifications we want to accomplish in this optimization bandwidth by using the S-parameters, already explained in Section 2.4 and defined specifically for this design in Section 3.6.

In terms of reflection we want both TE_{10} and TE_{01} to have fairly low return losses, and reasonably high transmission coefficients to their corresponding ports. Needless to say that all "inter-modal" parameters as well as parameters that relate our two single-mode ports should be even lower. Additionally, the ports should be long enough so that the higher-order modes that could be generated decay rapidly before they enter the different sections in our device. Summing up these requisites they can be described as

$$S_{1(1)1(1)}(\text{dB}),\ S_{1(2)1(2)}(\text{dB}),\ S_{2(1)2(1)}(\text{dB}),\ S_{3(1)3(1)}(\text{dB}) \leq -20 \text{ dB}$$

$$S_{2(1)1(1)}(\text{dB}),\ S_{3(1)1(2)}(\text{dB}),\ S_{1(1)2(1)}(\text{dB}),\ S_{1(2)1(2)}(\text{dB}) \geq -0.5 \text{ dB}$$

$$\text{Rest} \leq -60 \text{ dB}$$

Before jumping into further elaboration of the design, a reminder of the S-parameters properties applying to our device will be made. Our device is not reciprocal nor symmetrical, but it is, ideally, loss-free. For loss-free (passive) networks, transmitted and reflected power must be equal to incident power which translates into the equalities in section 2.4, $|S_{21}|^2 + |S_{11}|^2 = 1$ and $|S_{12}|^2 + |S_{22}|^2 = 1$. Thus, by setting the requisite we want to fulfill for the reflection coefficient of each mode, we are implicitly setting the limit for our transmission coefficient as well (an approximation has been made in the specifications above).

Another way to express these equalities is $[S]\,[S]^H = [I]$, where $[S]^H$ is the self-adjoint (or Hermitian) of the S-matrix and $[I]$ es the identity matrix. This equation entails that, ideally, for our device:

$$|S_{1(1)1(1)}| = |S_{2(1)2(1)}| \quad |S_{1(2)1(2)}| = |S_{3(1)3(1)}|$$
$$|S_{2(1)1(1)}| = |S_{1(1)2(1)}| \quad |S_{3(1)1(2)}| = |S_{1(2)3(1)}|$$

Note that we are using the module function in all the former statements, otherwise we would be assuming the reciprocity and symmetry of the device.

In the next steps of the design various simulations will be illustrated in which, curiously enough, these equalities might apparently not be fulfilled. However, the reader should keep in mind that this is due to accuracy limits in the simulations along with small numerical errors when it comes to calculating the parameters.

5.4 Input and output ports: considering higher-order modes

As we have said in the last section, we need to consider how long our ports should be in order to attenuate enough the higher-order modes that may generate at the input port. As we can see in table 5.1, the closest mode for the common waveguide port (square port) is the TE_{11}, with a cutoff frequency of 10.6 GHz. The following steps will help us to find a length that fulfills our requisites:

$$20\log(e^{-\gamma z}) = -60 \text{ dB} \tag{5.2}$$

$$z = \frac{\ln(10^3)}{-\gamma} \tag{5.3}$$

As the reader might have previously guessed, it all comes down to γ, the propagating constant, which is defined by:

$$\gamma = \sqrt{-\omega^2 \mu_r \mu_0 \epsilon_r \epsilon_0 + k_c^2} \tag{5.4}$$

$$k_c = \sqrt{\left(\frac{\pi m}{a}\right)^2 + \left(\frac{\pi n}{b}\right)^2} \tag{5.5}$$

Since the attenuation will be bigger the higher value of γ which, at the same time, will be bigger the lower the frequency goes, we need to make sure to check the worst case scenario, i.e., at the top frequency of our optimization bandwidth. Thus, with $f_{sup} = 9.5$ GHz, $m = n = 1$, and $a = b = 20$ mm, the following length is calculated:

$$\gamma = 98.52 \text{ 1/m} \quad z_{in} = 70 \text{ mm}$$

Now we will repeat the same process for the single-mode ports (WR90). This time the closest higher-order mode is TE_{20} so the parameters we use for equations 5.2 and 5.5 are $m = 2$, $n = 0$, $a = 22.86$ mm, and $b = 10.16$ mm:

$$\gamma = 189.482 \text{ 1/m} \quad z_{out} = 36 \text{ mm}$$

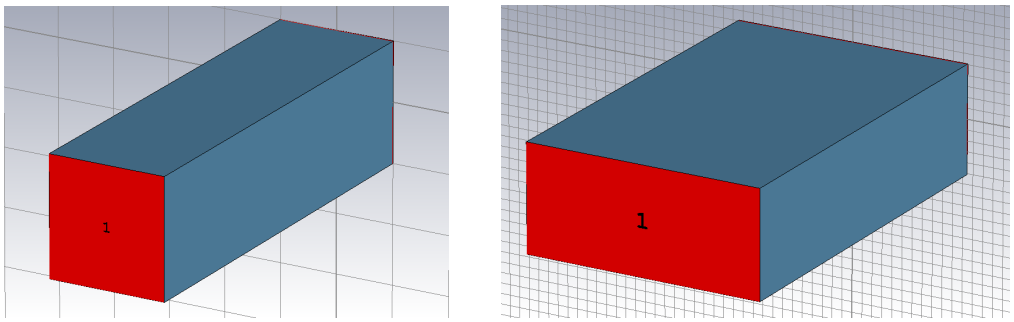

(a) Port 1. Input port. Square Waveguide.

(b) Port 2. Axial port. Rectangular Waveguide.

Figure 5.2: Ports of our OMT. Square waveguide (Port 1) and Rectangular waveguide (Port 2).

In order to verify this theoretical calculations, we will simulate independently each of the ports with CST Microwave Studio. Figure 5.2a and 5.2b show the physical structure of each of the ports whilst figure 5.3 shows the transmission coefficients of the higher-order modes in the waveguides. As expected, we have accomplished an attenuation of around 60 dB at the top frequency of our simulation bandwidth, 9.5 GHz.

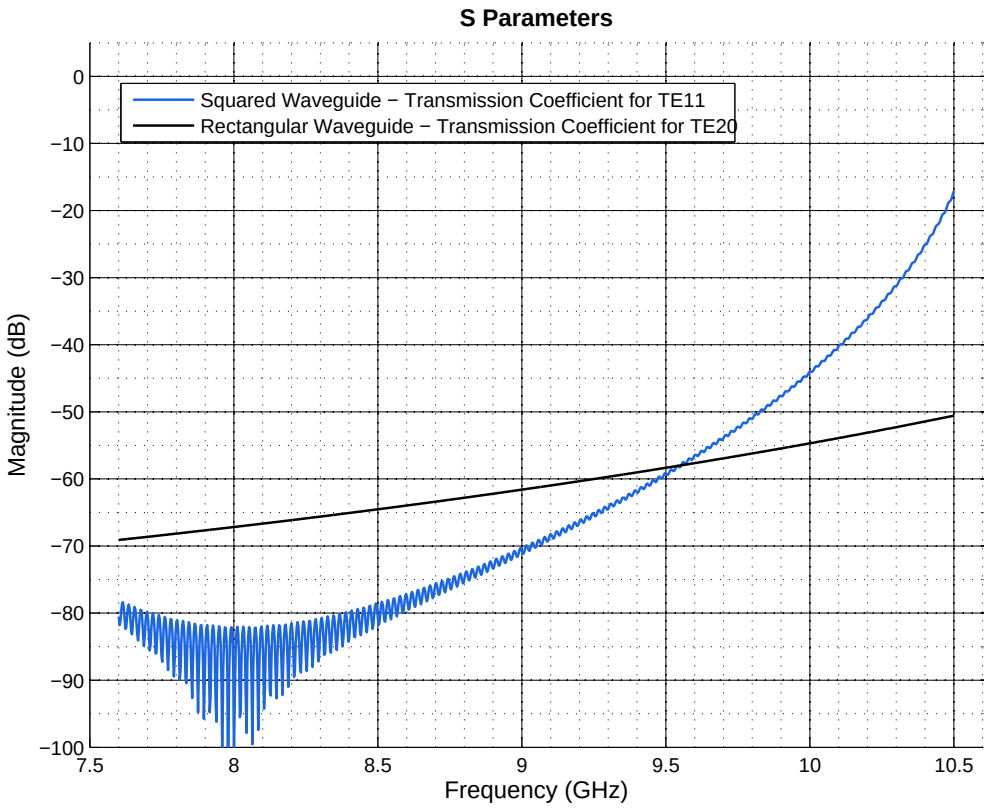

Figure 5.3: Simulated results of the ports by CST: Transmission coefficients of the higher-order modes.

5.5 Axial port matching: First approach

The next step in the design is to consider what waveguide interface it is going to be used to transition from the common square waveguide to the axial port. After some tests, we decide to use stepped waveguide transformers. A number of possibilities now arise, we need to choose how many transformers are we going to use as well as how many symmetries are they going to hold regarding the common waveguide port.

As first attempt, and since the width and height of the two ports we need to adapt are different, we will use the *Uher method* ([6]) to calculate the parameters of the transformer sections (width, height and length). In order to perform these calculations a simple MATLAB code has been developed. The input arguments for this program are the dimensions of both input and output ports, the number of $\frac{\lambda}{4}$ transformer sections, the relative permittivity of the dielectric inside the waveguide (air in this case), the waveguide's wavelength (λ_g), and the center operating frequency. Table 5.2 shows the results of running this program with four transformer sections.

	Width (a)	**Height** (b)	λ_g	**Length**
Transf. 1	20.5 mm	19.4 mm	56.2 mm	14.0 mm
Transf.2	21.1 mm	16.3 mm	53.6 mm	13.4 mm
Transf. 3	21.7 mm	12.9 mm	51.5 mm	12.9 mm
Transf. 4	22.3 mm	10.7 mm	49.7 mm	12.4 mm

Table 5.2: Uher method output values for stepped waveguide transformers.

Introducing these parameters in CST, the simulation of the structure illustrated in figure 5.4.

During this simulation we specify certain boundary conditions. A PMW in the yz plane was introduced with CST MS in order to ignore the TE_{01} for the moment being. The S-parameters regarding the transmission of the TE_{10} mode through the common port to the axial port are shown in figure 5.5.

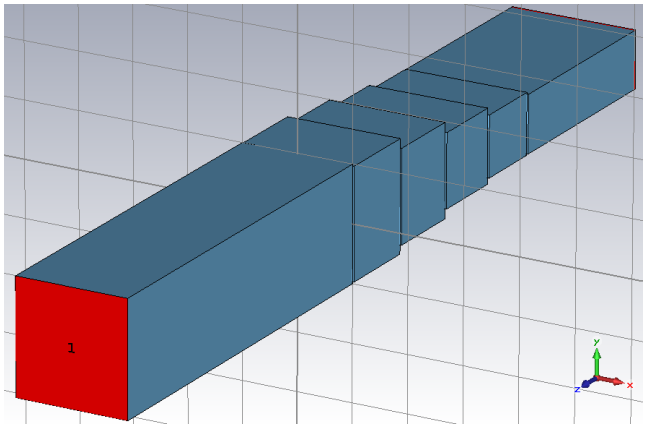

Figure 5.4: Structure with four $\frac{\lambda}{4}$ transformer sections calculated through the Uher Method.

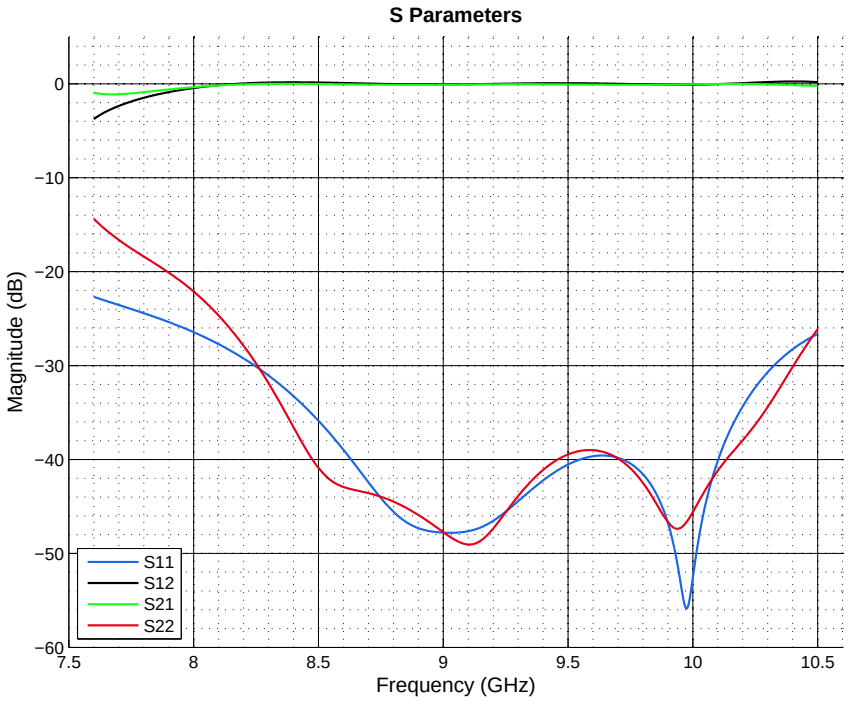

Figure 5.5: Simulated results by CST: S-parameters of the axial structure.

Up to this point the structure seems to be fulfilling the specifications set in Section 5.3, so the next step in the design is the addition the branching waveguide.

5.6 Branching Port: Irises and Septum

The branching or lateral port will be a WR90 rectangular waveguide just like the axial port. As mentioned while explaining taper/branching OMT types in Section 3.3.1, it is known that in this type of devices the branching waveguide port is generally constructed along with one or more *inductive irises* (i.e., a symmetric H-plane discontinuity, see figure 2.2a). These irises help to coupling the TE_{01} mode of the common port with the fundamental mode, TE_{10}, of the branching port (i.e., the H_z field of the TE_{01} mode is coupled to the H_x field of the fundamental mode of the branching port). They yield a smaller rectangular aperture size and thus, improved matching properties of the longitudinal single signal port.

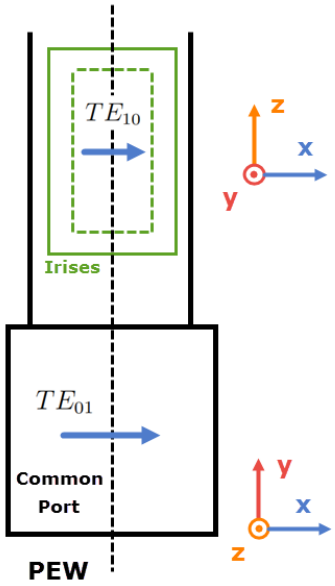

Figure 5.6: Diagram of the branching (lateral) port and the TE_{01} coupling.

Also, as we explained in former sections, the location of the branching waveguide is of critical importance, especially for the performance of the rectangular TE_{01} mode. It should be placed with a location such that the TE_{01} mode can propagate adequately to the common port, while becoming evanescent within the stepped region to not compromise the path dedicated to the TE_{10}. Additionally, the inclusion of a septum section can very decisively help with this last task as well. The general location of this structures is shown in figure 5.6 and figure 5.7.

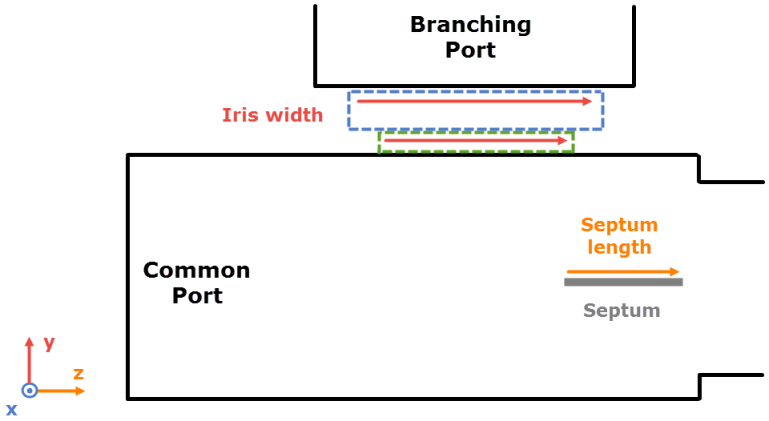

Figure 5.7: Lateral of the branching port and septum location.

From this point forward, the optimizer functionality of the CST MS will prove to be very helpful, since it will calculate the most optimal parameters (dimensions and location of this structures) that fulfill our specifications.

In order to do that, we need to express our requisites in form of a *cost function*. Fortunately for us, this is fairly simple thanks to CST MS interface, where we just need to specify what value of which S-parameters we want to achieve along with the optimization algorithm (specified in 4.2). For the moment being, the goals will be set for the return losses of each mode to be, at maximum, -20 dB. This will lead to a cost function of the form:

$$F_{cost} = \sum_{i=f_{inf}}^{fsup} [W_1(S_{1(1)1(1)} - S^1_{goal}) + W_2(S_{1(2)1(2)} - S^2_{goal})]$$

where S^1_{goal} and S^2_{goal} are the reflection coefficients of each mode respectively, and W_1 and W_2 are weight coefficient for each goal. Both goals will weight the same for now.

However, due to the nature of numerical optimization, the initial value of the parameters is essential. This results from different ideas: first, the closer the initial value is to the most optimal solution, the faster the process is going to be; and secondly and most importantly, in the worst case scenario, the optimization loop might not converge.

Thanks to the information explained in the first paragraph, we know that the branching port should most probably be placed around a location close to the start of the stepping transformer region, thus propagating correctly between the desired ports (common and branching ports) but, at the same time, becoming evanescent right after, and so having the minimum possible effect in the longitudinal signal path. In terms of the septum location, as explained in section 3.3.2, it should be placed right after or partially overlapping the branching waveguide. This positioning will result in a section being seen as two regions of half height in terms of TE_{01}, becoming reflected and coupled to the branching port. This initial configuration is shown in figure 5.7.

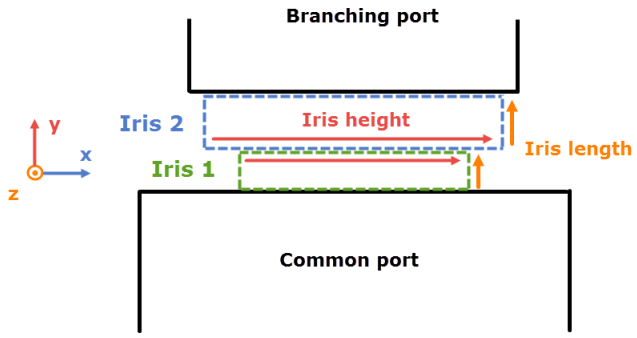

Figure 5.8: Cross-section diagram of the branching port and irises.

Now we will run the optimization entering the following parameters to optimize:

- Lateral port's and irises's location (along the z coordinate).
- Iris 1: Width and height.
- Iris 2: Width, height and length.
- Septum: Position (y and z coordinates) and length (along the z coordinate).

Note that we have not entered iris one's length nor septum width (along the y coordinate). The reason for this is that both these dimensions will tend to decrease to the minimum possible value so, as a manufacturing accuracy limit, we will set both this parameters at 0.5 mm.

Figure 5.9 illustrates the structure resulting from this first optimization.

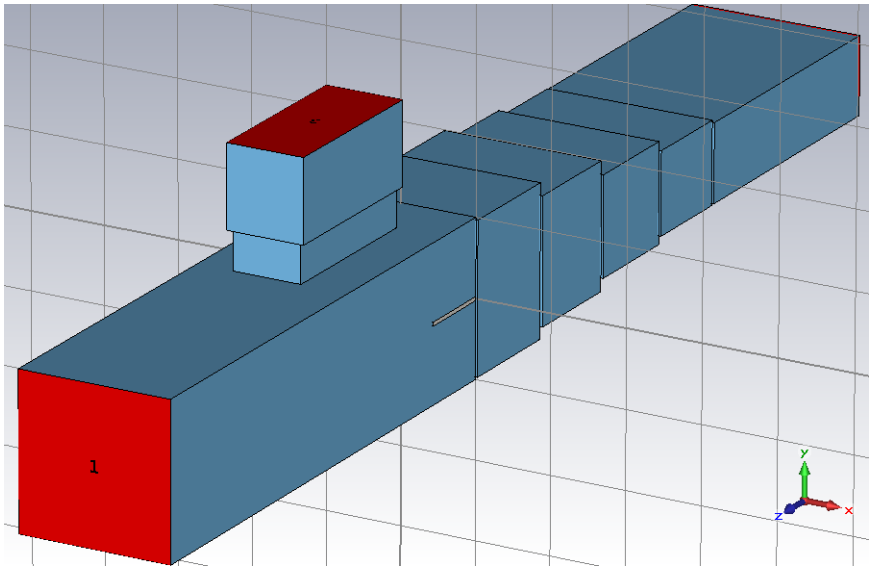

Figure 5.9: OMT design after first optimization.

The S-parameters resulting from the simulation with the optimized values are plotted in figure 5.10.

Note that the all "inter-modal" parameters along with the parameters that relate axial and branching ports between them do not appear in the figure. This absence of some S-parameters will be repeated in the upcoming plots and it is mainly for clarity reasons, since all of them are low enough to satisfy our initial requisites.

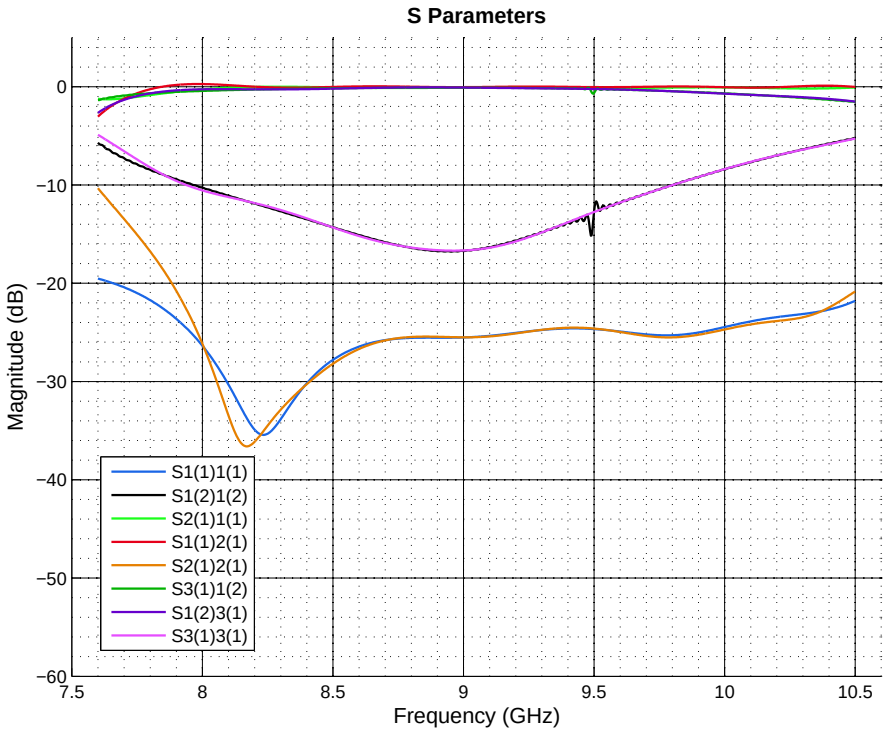

Figure 5.10: Simulated results of the OMT by CST: S-parameters after first optimization.

Unfortunately, as it can be seen in the S-parameters representation, the reflection coefficients of the horizontal mode TE_{01} are nowhere near the -20 dB, and in fact, they are fairly far of achieving our requisites. Moreover, looking closely to these parameters a small disturbance can be noticed in $S_{3(1)1(2)}$ and $S_{1(2)1(2)}$. This is generated by a resonant cavity, and this phenomenon will be explained and dealt with during the next section.

5.7 Undesired resonances and optimization process

A resonant cavity is a region of dielectric material totally or partially limited by some sort of conductor surface in which standing waves can be built up. This phenomenon is deliberately used in various devices such as resonators or resonant accelerators. However, it can also be created accidentally in waveguide structures when, due to different circumstances, electromagnetic waves are reflected at the propagation direction, giving rise to the standing-wave patterns of a resonance.

The first step to deal with an undesired resonance is to see how the electromagnetic field is behaving at that frequency. In order to see that we can use CST's FS (Frequency Solver), and place a field monitor at that exact frequency. After running a simulation of the structure in 5.9 with the FS and narrowing the simulation bandwidth for more accuracy, we can see that this resonance is located at 9.5215 GHz. We will proceed now to place a field monitor to see how the fields are behaving at that frequency. This process is shown in figure 5.11.

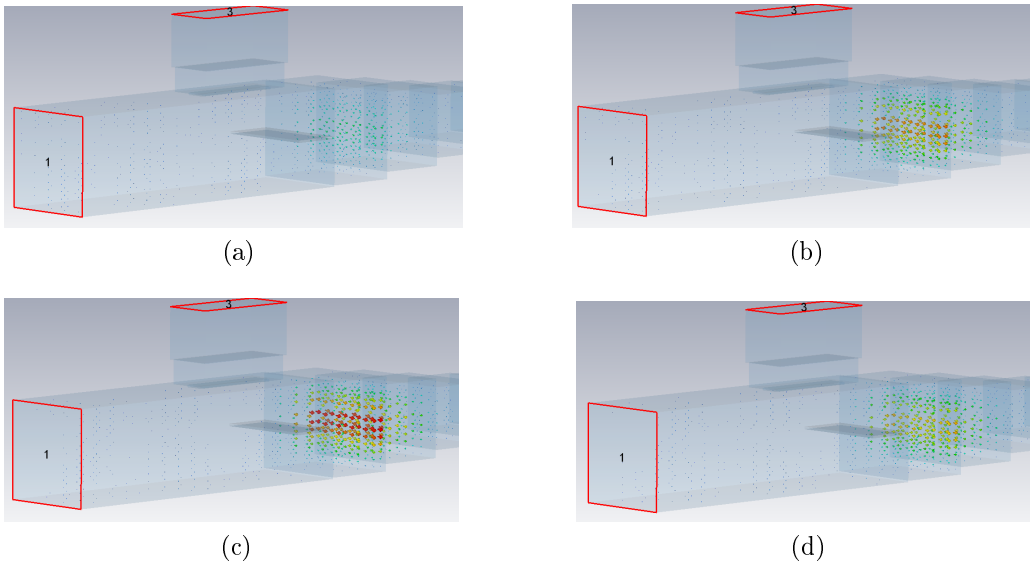

Figure 5.11: Simulated results by CST: Field monitor for the TE_{10} at 9.5215 GHz.

The first thing to notice when looking at the field monitor is that the magnitude of the field moving through the input port in comparison with the field right after the septum is incredibly small.

Therefore, what is happening in this situation is that, for whatever reason, the TE_{01} is not becoming evanescent soon enough, enclosing the field into the first transformer section. The field is unable to propagate in either direction of the device and keeps getting reflected over and over, creating an standing-wave.

The analysis of this resonance makes us realize that, up to this point, we had only optimize the iris and septum while completely overlooking the transformers impact in our structure. Even though these transformer sections were calculated to improve the adaptation of the vertical mode, they are also affecting the horizontal mode and the behavior of the structure overall.

Additionally, prior to this point in the design we had been holding symmetry with respect to both xz plane and yz plane in out transformer sections. However, we could have even more degrees of freedom in our design if we remove the xz plane symmetry and therefore, being able to add the center of our transformer sections and the center of the axial port to the optimization process.

To sum up, these will be the parameters to enter in the optimization this iteration:

- Iris 1: Width and height.
- Iris 2: Width, height and length.
- Transformers: Length, height and centers (y coordinate).
- Axial port center (y coordinate).
- Septum: Position (y and z), length (along the z coordinate).

The results from this optimization are illustrated in figure 5.12 and 5.13.

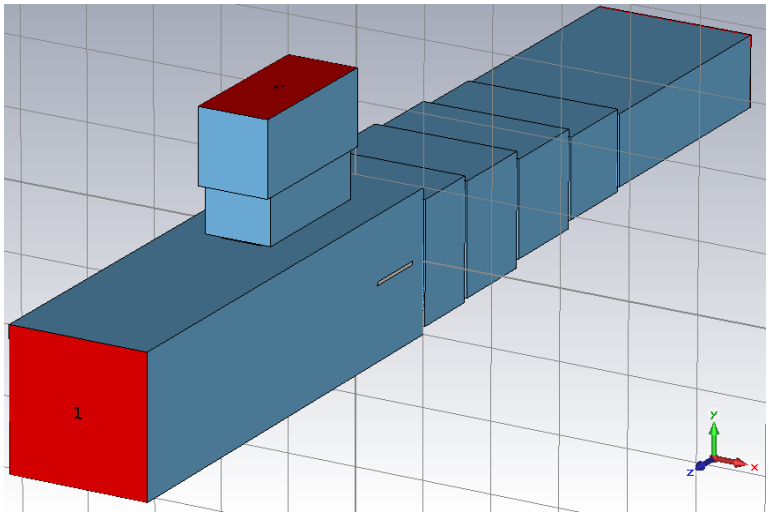

Figure 5.12: OMT design after second optimization.

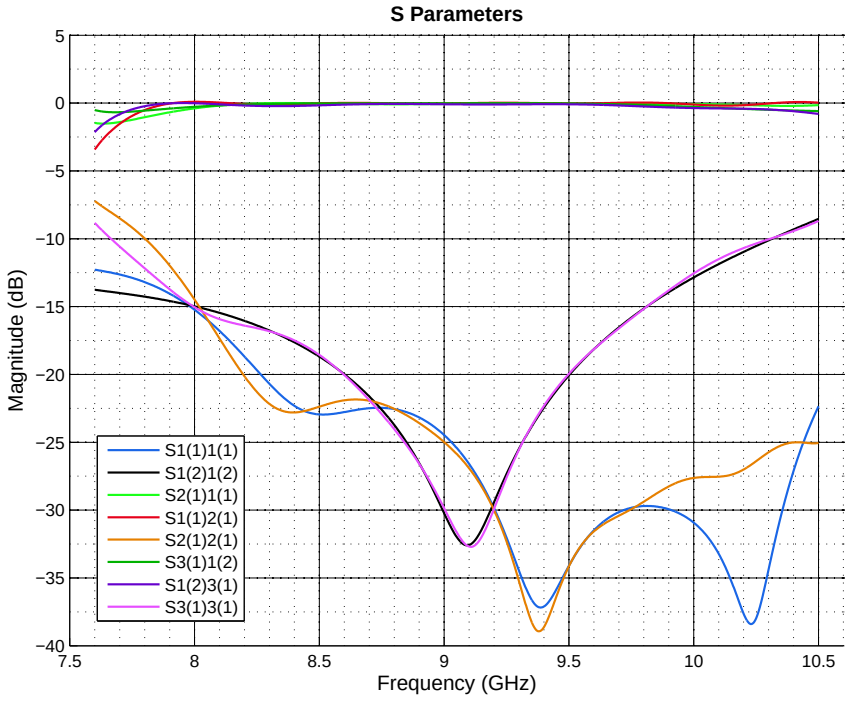

Figure 5.13: Simulated results of the OMT by CST: S-parameters of the design after second optimization.

As it can be seen in figure 5.13, the addition of the transformer dimensions to the optimization parameters has definitely paid off. The reflection coefficients of both vertical and horizontal mode greatly improved up to the point where our specifications are now satisfied in the bandwidth from 8.6 to 9.5 GHz.

Now, in order to achieve a bandwidth a little bit wider we will come back to our cost function and increase the weight of the horizontal mode (W_2). This will prioritize the fulfillment of our second goal (reflection coefficient of horizontal mode) over our first goal (reflection coefficient of vertical mode) during the optimization process. Setting W_2 to exactly double W_1 we get the following results.

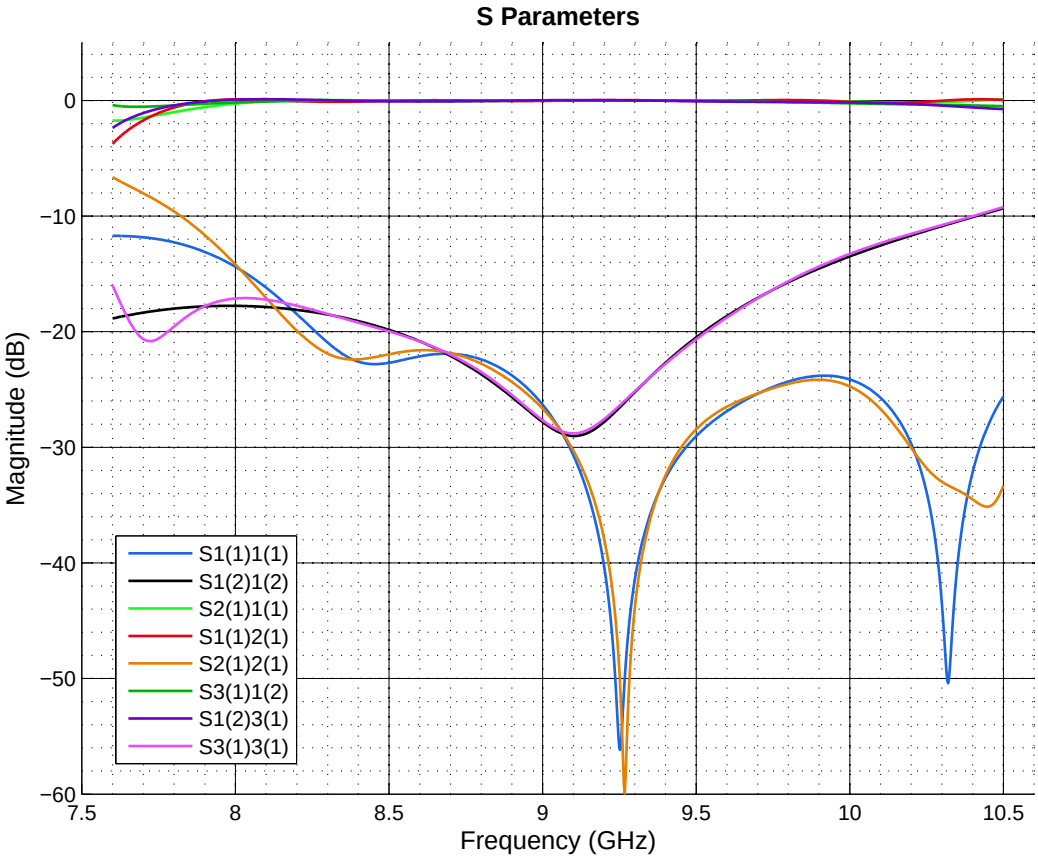

Figure 5.14: S-parameters of final design of the OMT.

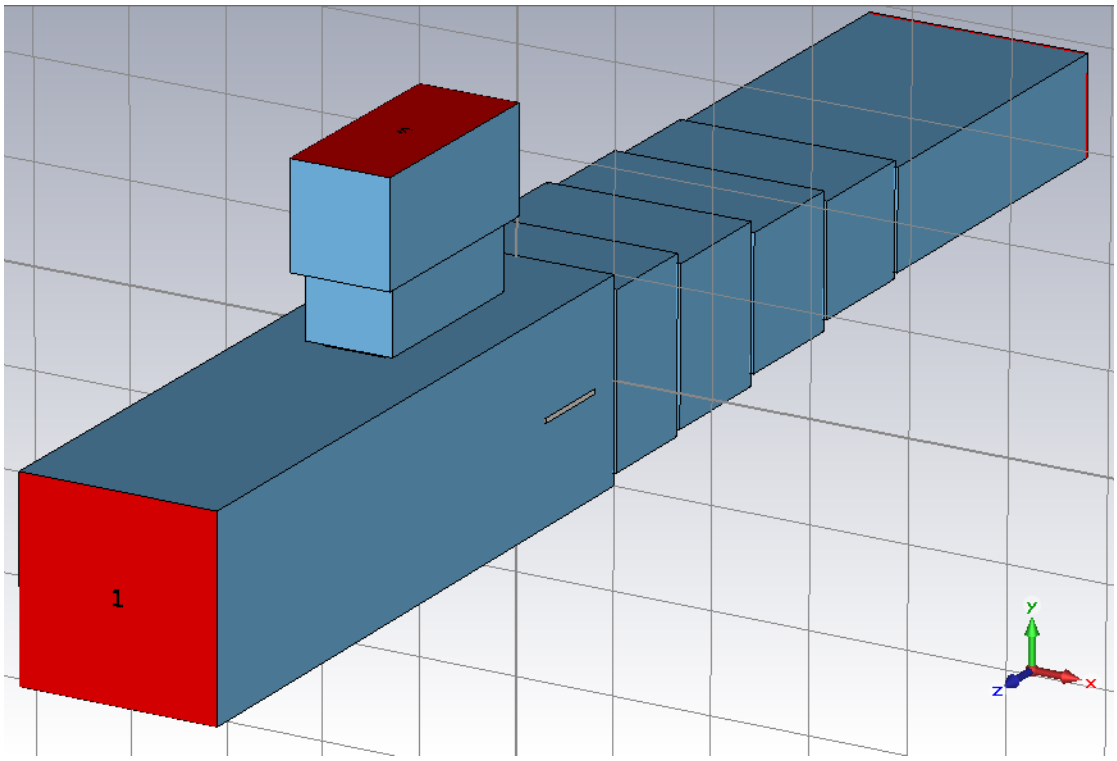

Figure 5.15: OMT design, final optimization.

Finally, the design coming out of this last optimization fulfills all our specifications, maintaining all the reflection coefficients below -20 dB between 8.5 and 9.5 GHz. Needless to say that, again for clarity reasons, all "inter-modal" parameters along with the parameters that relate axial and branching ports between them do not appear in the figure; however, they are way below the specifications (around -100 dB).

The finals values of the parameters that define the structure in figure 5.15 can be found in Appendix B.

As the last step, we will simulate this final design with the Frequency Solver as well, since it presents a more accurate representation in the frequency domain.

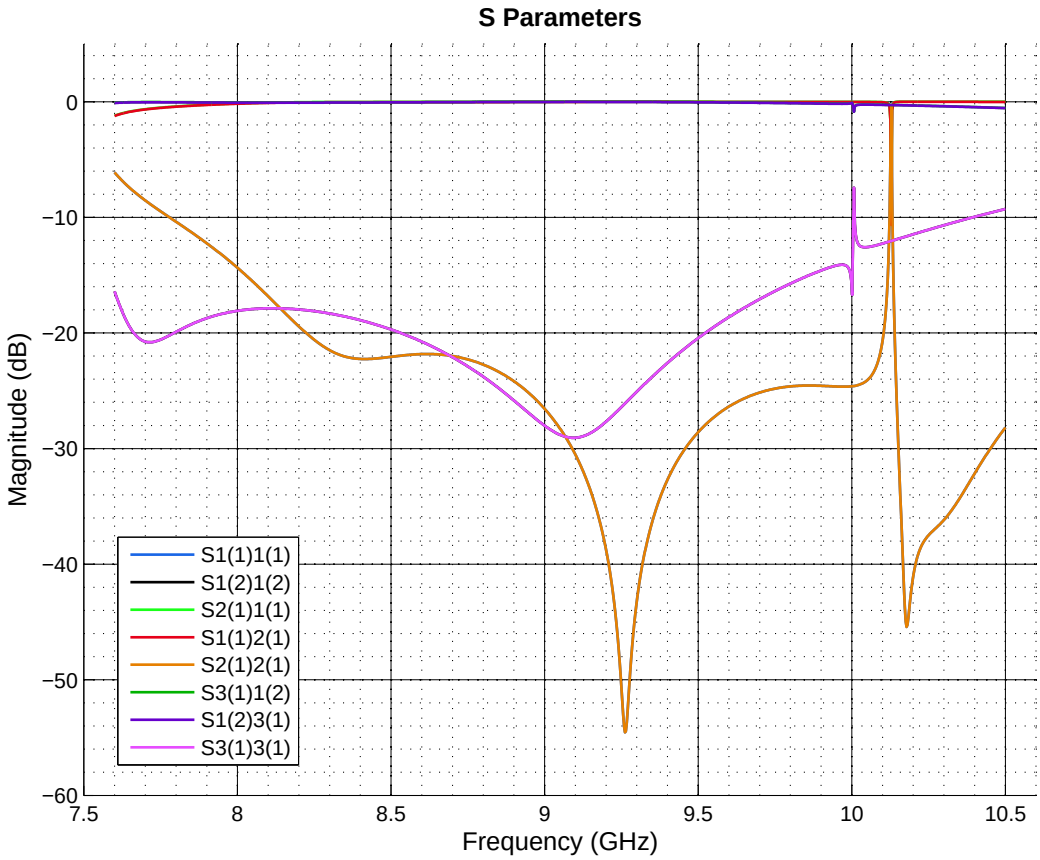

Figure 5.16: Simulated results of the OMT by CST: S-parameters of the final design of the OMT. Frequency Solver.

Figure 5.16 shows a couple of things that are worth to mention. First, due to this more accurate representation the reflection and transmission coefficients of each mode are completely overlapped (i.e. the pairs $S_{1(1)1(1)}$ - $S_{2(1)2(1)}$, $S_{1(2)1(2)}$ - $S_{3(1)3(1)}$, $S_{1(1)1(1)}$ - $S_{2(1)2(1)}$, $S_{2(1)1(1)}$ - $S_{1(2)2(1)}$, and $S_{3(1)1(2)}$ - $S_{1(2)3(1)}$), as it should be for a loss-less network.

Also a couple of resonances have appeared above the 10 GHz mark. However, since these resonances are outside our optimization bandwidth, they will be overlooked for the moment being. Their effect and how to remove them should be approach in a future work of the project.

5.8 Convergence Analysis

All the former simulations and optimizations have been run under the same precision, i.e. 15 lines per wavelength, which builds a discretization mesh of 104.545 cells (details of this type of simulation were explained in section 4.2). However, in order to check the convergence of our solution we will run simulations with a more dense mesh, therefore making sure that the approximations done during the simulation process have not affected our results very heavily.

The importance of convergence should not be underestimated. Both simulation and optimization are iterative processes and, by definition, values are changing from one iteration to the next. If this change is significant then that means the results we are relying upon for our decision making are changing significantly as well. Sometimes it might be obvious and an non-converged solution will show fictitious results but we surely need to be cautious about this. Now, we will run simulations of our structure with 20, 22 and 25 lines per wavelength, which will build a discretization mesh of 190060, 222075 and 282240 discretization mesh respectively. The next group of figures illustrates the variation of some of the S-parameters with the different precision.

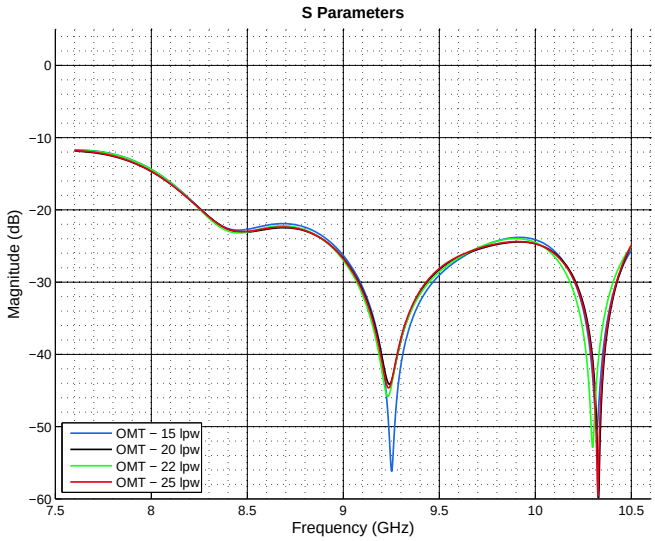

Figure 5.17: Simulated results of the OMT by CST: Reflection coefficient of the Vertical mode.

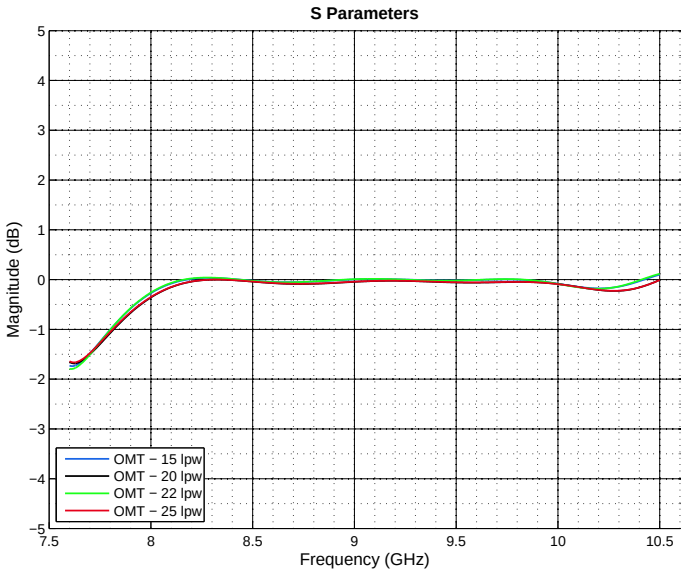

Figure 5.18: Simulated results of the OMT by CST: Transmission coefficient of the Vertical mode.

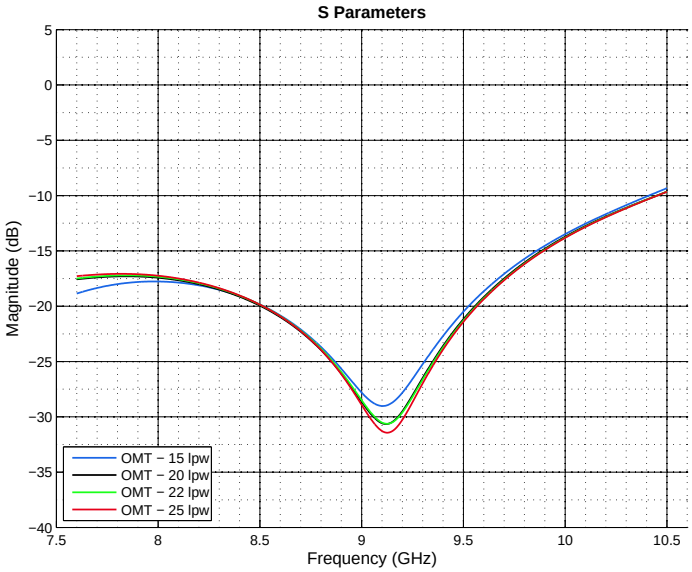

Figure 5.19: Simulated results of the OMT by CST: Reflection coefficient of the Horizontal mode.

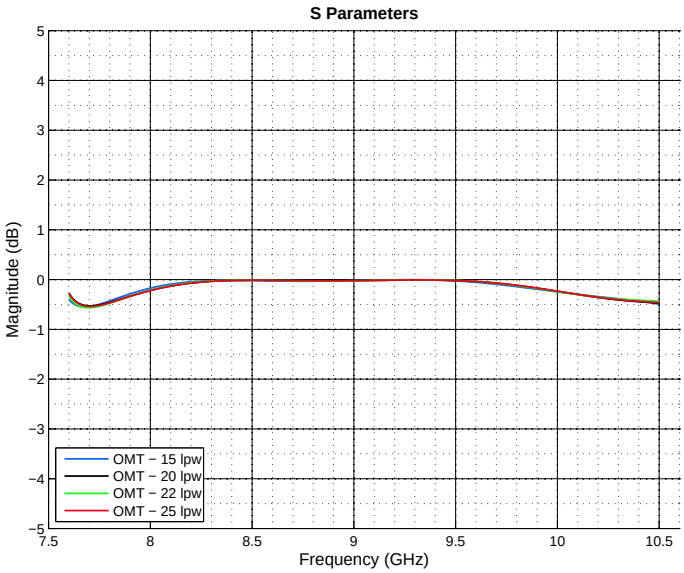

Figure 5.20: Simulated results of the OMT by CST: Transmission coefficient of the Horizontal mode.

Fortunately, the disparity between the plots of different precision is minimum, and with this we can assume that our solution for Maxwell's equations in our design is adequate.

5.9 Conclusions

The whole design process has been presented in this chapter, leading to the final form of the OMT.

As a first approach, a simple design was built with the help of the theory described in the previous chapters. However, various iterations of optimization have been required to achieve the final design, which fulfills the initial specifications set in this chapter. During these iterations the parameters to optimize have been changing in order to remove undesired phenomenons in the structure (resonances). Finally, an analysis of convergence has been carried out.

Nonetheless, our final design is far from perfect and, as a matter of fact, some resonances are still present outside of our optimization bandwidth. As

a result of these flaws, a small section regarding the possible future work will be presented along with a summary of the whole project as the last chapter of the document.

Chapter 6

Final Conclusions and Future Work

6.1 Final conclusions

Throughout this project a design of a narrowband ortho-mode transducer in rectangular waveguide technology has been developed.

The progression during this work can be divided into 3 main parts: study of electromagnetic theory, research of OMT structures and their operating, and the application of these concepts into the design process itself.

Electromagnetic theory relating to the rectangular technology was presented prior to the actual design. The good comprehension of certain concepts such as symmetries within rectangular waveguides, i.e. PMW (Perfect Magnetic Wall) and PEW (Perfect Electric Wall) or the understanding of higher-mode generation was essential in order to build a solid base to follow the design process.

After that, a survey of different configurations of OMTs was presented. Although the extension of this study was longer than what was strictly necessary (because of the addition of Wideband OMTs), the review of the many designs had the intention to give the reader a great insight about ortho-modes and how they work.

All the knowledge gathered throughout the first stages of the project allowed us to approach the first design. In order to do this, the first step

was to calculate the ports dimensions and to adapt the axial signal path (i.e. TE_{10} mode). The adaptation was achieved through four transformer sections that were calculated through the Uher method. As the next step we added the branching or lateral port along with two irises and a septum region, just as it had been explained in the respective configurations of OMT during the former survey.

At this point, an optimization cycle took place. Even though various optimizations were made during the design process, only the three major ones are described in this document. This is mainly because the rest of them served more as a learning progression, but without showing any real improvement in the design. For each of these optimizations the selection of parameters played a fundamental role along with the goals set in the optimizer.

In the first trial only the parameters regarding branching port placement, irises and septum were used. Unfortunately, this optimization lead to a structure that didn't satisfy our initial specifications and, as a matter of fact, introduced resonances into our operating bandwidth. Due to these resonances, it was decided to add the transformers parameters to the optimization as our next approach, leading to a simulation with much better results.

Finally, after a small tweak in our optimization goals we achieved a design that fulfilled all of our specifications within the desired bandwidth.

6.2 Future work

The design is clearly open to further improvement and research.

A careful study of the resonances created outside of the optimization bandwidth would allow us to reach a further understanding of the fields inside the device and, most probably, help us figuring out new approaches and technologies to use in order to improve the performance over the operating bandwidth.

Additionally, there was no opportunity to manufacture the final design and, thus, present actual measures from the physical device. It would be very interesting to compare simulated with measured results, and keep an eye in to what extent the real return losses and transmission coefficients are similar to the computed values.

Bibliography

[1] D.M, Pozar, "Microwave Engineering", Fourth Edition, John Wiley & Sons Inc., 2012.

[2] Robert E. Collin, “Foundations for Microwave Engineering”, Second Edition, John Wiley & Sons Inc., New York, 2001.

[3] N. Marcuvitz, “Waveguide Handbook”, New York, Dover Publications, Inc., 1951.

[4] A.M. Bøifot, E. Lier and T. Schaug-Pettersen, “Simple and broadband ortho-mode transducer (antenna feed)”, IEE Proceedings H Microwaves, Antennas and Propagation, vol. 137, nº. 6, pp. 396-400, Dec. 1990.

[5] A.M. Bøifot, “Classification of Ortho-Mode transducers”, Europ. Trans. Telecom. and Related Technologies, vol. 2, nº. 5, pp. 503-510, Sept. 1991.

[6] J.Uher, J. Bornemann and U. Rosenberg, “Waveguide components for antenna feed systems: Theory and CAD”. Boston, Artech House, 1993.

[7] J. A. Ruiz-Cruz, J. R. Montejo-Garai, J. M. Rebollar, “Full-Wave Modeling and Optimization of Bøifot Junction Ortho-Mode Transducers”, Int. J. RF Microw. Comput.-Aided Eng., 18, 4, pp. 303-313, Julio 2008.

[8] Ignacio Izquierdo Martinez, “Design of wideband orthomode transducers based on the turnstile junction for satellite communications”, Proyecto Fin de Carrera, Universidad Autónoma de Madrid, Nov. 2008.

[9] Press, WH; Teukolsky, SA; Vetterling, WT; Flannery, BP. "Downhill Simplex Method in Multidimensions". Numerical Recipes: The Art of Scientific Computing (3rd ed.). New York: Cambridge University Press, 2007.

Appendix A

Symmetry planes of TE/TM modes

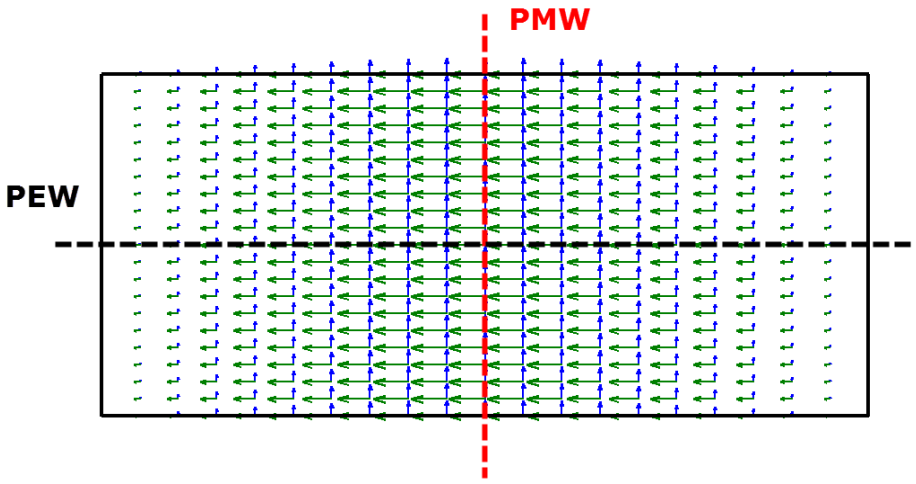

Figure A.1: TE10 mode of a rectangular waveguide.

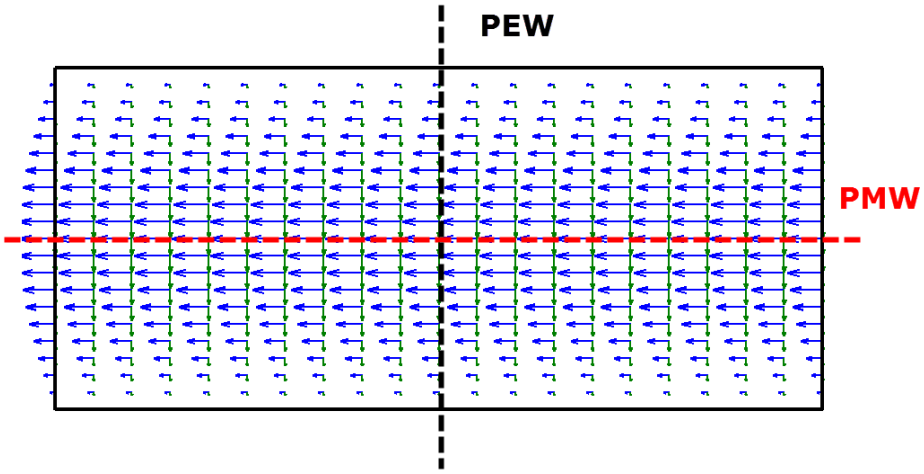

Figure A.2: TE10 mode of a rectangular waveguide.

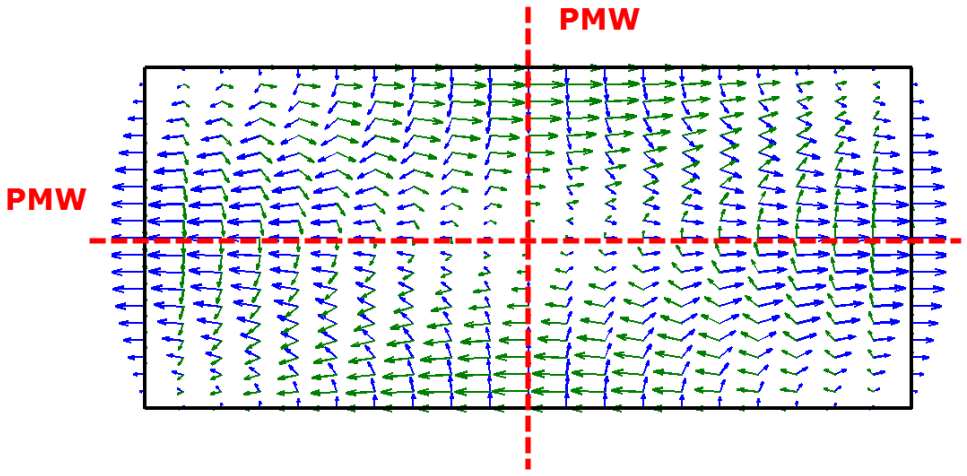

Figure A.3: TE11 mode of a rectangular waveguide.

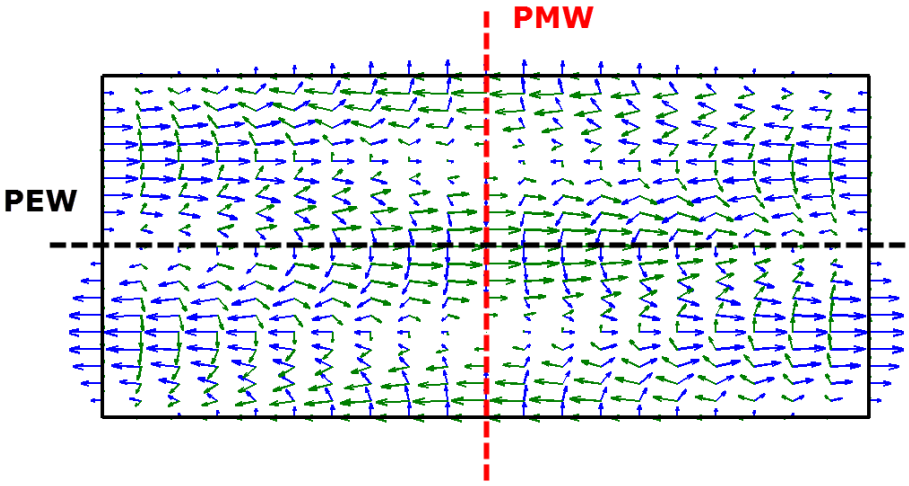

Figure A.4: TE12 mode of a rectangular waveguide.

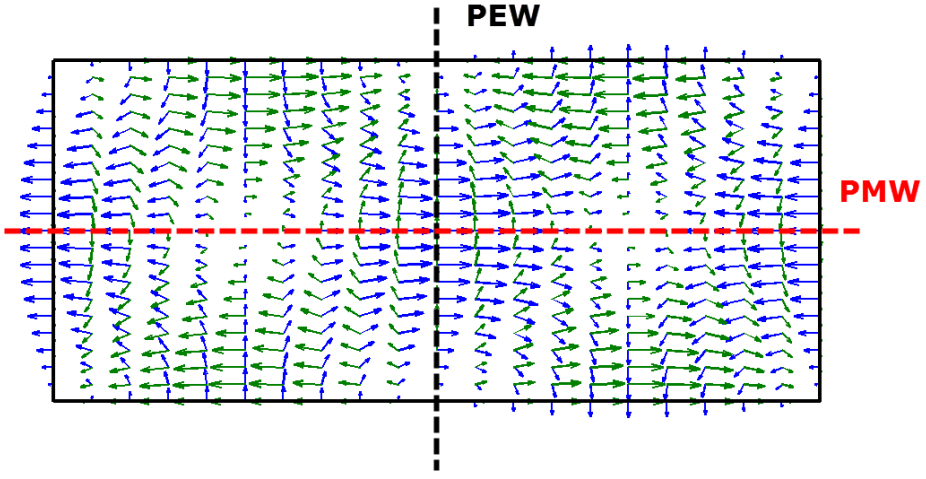

Figure A.5: TE21 mode of a rectangular waveguide.

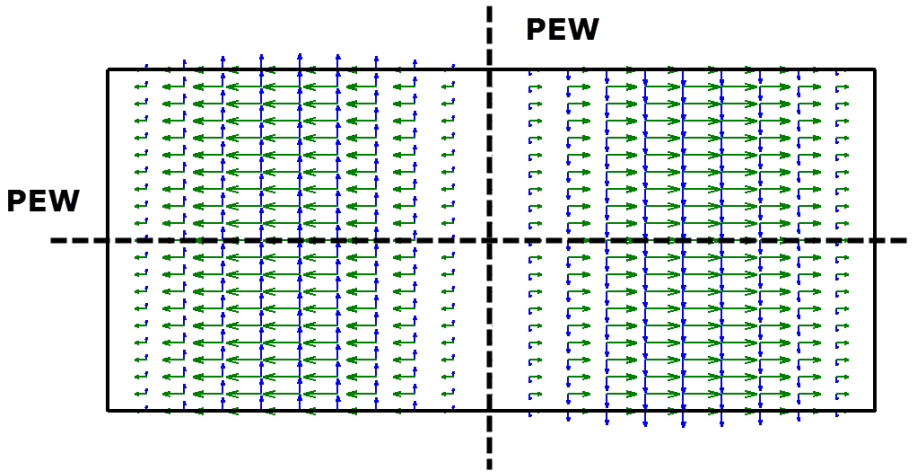

Figure A.6: TE20 mode of a rectangular waveguide.

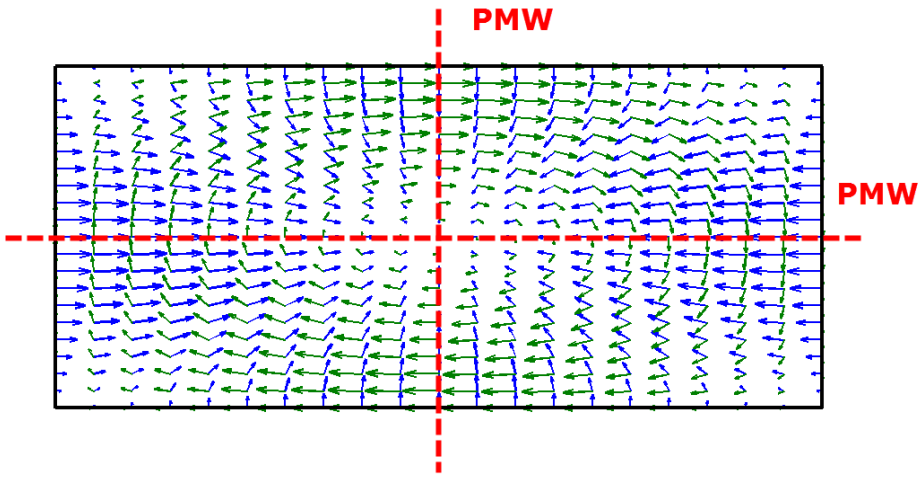

Figure A.7: TM11 mode of a rectangular waveguide.

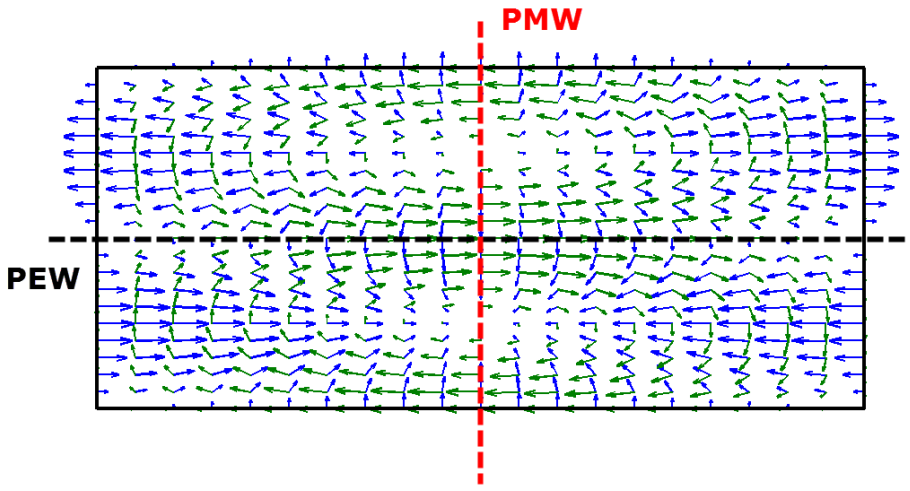

Figure A.8: TM12 mode of a rectangular waveguide.

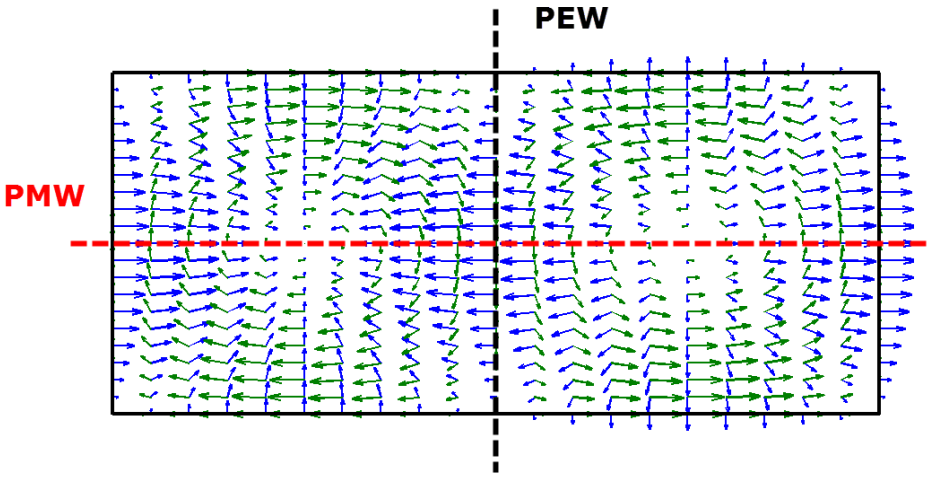

Figure A.9: TM21 mode of a rectangular waveguide.

Appendix B

List of parameters of the Ortho-Mode final design

Common Port	**Description**	**Value(mm)**
a_i	Width (x coordinate)	20
b_i	Height (y coordinate)	20
z_{in}	Length (z coordinate)	70

Table B.1: Dimensions of the common (square) port. OMT final design, figure 5.15.

Axial Port	**Description**	**Value(mm)**
a_o	Width (x coordinate)	22.86
b_o	Height (y coordinate)	10.16
z_{out}	Length (z coordinate)	36
$axcenter$	Center position (along y coordinate)	0.062

Table B.2: Dimensions of the axial (WR90) port. OMT final design, figure 5.15.

Branching Port	**Description**	**Value(mm)**
a_{lat}	Width (z coordinate)	22.86
b_{lat}	Height (x coordinate)	10.16
z_{lat}	Length (y coordinate)	12
$zcenter$	Position (along z coordinate)	20

Table B.3: Dimensions of the lateral (WR90) port. OMT final design, figure 5.15.

Irises	**Description**	**Value(mm)**
$airis_1$	Width (z coordinate)	17.805
$airis_2$	Width (z coordinate)	19.752
$biris_1$	Height (x coordinate)	6.217
$biris_2$	Height (x coordinate)	8.900
$ziris_1$	Length (y coordinate)	0.5
$ziris_2$	Length (y coordinate)	6.761

Table B.4: Dimensions of the two irises used in the branching (WR90) port. OMT final design, figure 5.15.

Septum	**Description**	**Value(mm)**
$scentery$	Position (along y coordinate)	0.055
$scenterz$	Position (along z coordinate)	7.846
$zseptum$	Length (z coordinate)	8.893
$xseptum$	Width (x coordinate)	20
$yseptum$	Height (y coordinate)	0.5

Table B.5: Dimensions of the septum placed inside the common port. OMT final design, figure 5.15.

Transformers	**Description**	**Value(mm)**
atr_1	Width transformer 1 (x coordinate)	20.5
atr_2	Width transformer 2 (x coordinate)	21.1
atr_3	Width transformer 3 (x coordinate)	21.7
atr_4	Width transformer 4 (x coordinate)	22.3
btr_1	Height transformer 1 (y coordinate)	17.390
btr_2	Height transformer 2 (y coordinate)	15.737
btr_3	Height transformer 3 (y coordinate)	13.471
btr_4	Height transformer 4 (y coordinate)	11.375
ltr_1	Length transformer 1 (z coordinate)	11.038
ltr_2	Length transformer 2 (z coordinate)	12.954
ltr_3	Length transformer 3 (z coordinate)	12.917
ltr_4	Length transformer 4 (z coordinate)	12.675
$trcenter_1$	Position transformer 1 (along y coordinate)	-0.073
$trcenter_2$	Position transformer 2 (along y coordinate)	-0.185
$trcenter_3$	Position transformer 3 (along y coordinate)	-0.066
$trcenter_4$	Position transformer 4 (along y coordinate)	0.045

Table B.6: Dimensions of the four transformers in the tapper section of the longitudinal path. OMT final design, figure 5.15.